Report
P-20-26
May 2021

Ion composition at bentonite-water interface and its impact on erosion

Ivars Neretnieks
Luis Moreno

SVENSK KÄRNBRÄNSLEHANTERING AB

SWEDISH NUCLEAR FUEL
AND WASTE MANAGEMENT CO

Box 3091, SE-169 03 Solna
Phone +46 8 459 84 00
skb.se

SVENSK KÄRNBRÄNSLEHANTERING

ISSN 1651-4416
SKB P-20-26
ID 1920560
May 2021

Ion composition at bentonite-water interface and its impact on erosion

Ivars Neretnieks, Luis Moreno
Royal Institute of Technology, KTH

Keywords: Montmorillonite gel, Phase separation, Fracture clogging, Sol stability.

Abstract

In the KBS-3 design used in Sweden and Finland for a nuclear waste repository the waste canisters are surrounded by compacted bentonite clay. The clay protects canisters from mechanical shear, limits the intrusion of corrosive agents and slows down radionuclide escape, should the canister be damaged.

Groundwater seeping in the fractured crystalline rock at repository depth at present has ion concentration well above the critical coagulation concentration, CCC, above which the main mineral, the swelling montmorillonite, forms gel. Gel does not release colloidal particles either spontaneously or due to shear by the seeping water in the fractures. There are concerns that if waters below CCC in the future intrude the repository, the montmorillonite will disperse as sol and be carried away by the seeping water or by sedimentation in sloping fractures. Below-CCC waters can result from melting ice during and after ice ages but could also be increasingly generated by precipitation that displaces the underground water, even without ice ages. Over long times below-CCC water flow can erode non-negligible amounts of clay.

However, fractures can possibly be clogged. The detritus particles always present in natural bentonites could form filters either at the mouth of the fractures or within the variable aperture fractures. Experiments have shown that this can enormously slow down montmorillonite loss. Clogging by detritus has not been invoked as an argument in the safety analysis presented by the Swedish and Finnish companies, SKB and Posiva, respectively, responsible for the long-term performance assessment of the waste repositories.

It has also recently been found that phase separation of montmorillonite (mmt) sols forms strong complex agglomerates that within weeks to months form gel with yield strengths on the order of a few to many tens of Pa. The sediments may slow down further extrusion of clay into fractures.

Highlights

1. mmt sol is not stable. “Rapid” phase separation takes place.
2. Gel will slow down swelling rate of expanding compact bentonite into fractures.
3. Bentonite accessory minerals clog fractures.
4. Erosion and loss of bentonite barriers in fractured rock will be small.

Summary

In a KBS-3 type of repository, water flowing in fractures will carry ions to the interface of seeping water and bentonite that expands from the deposition hole. We have studied how the conditions at the clay water interface are influenced by that in the original clay and in different groundwater compositions and by the ion diffusion in the clay and between groundwater and clay at the interface.

The water seepage rate, the concentration of different ions at the interface and the mass transfer over the interface and in the clay itself determines the composition of the ions in the ion exchange positions in the smectite at the interface. This in turn determines if the smectite can solubilise and form a sol that can be carried away or if the smectite will collapse to microscopic stacks, aggregates, that sediment.

There is a narrow window of water compositions in which the smectite can solubilise. The water must be dilute, less than some 10–30 mM for this to happen, (< 0.02 % by weight salt). This is the critical coagulation concentration CCC. In seeping waters, the smectite particles can form flocs, which can sediment in sloping fractures. The flocs can re-solubilise in stagnant waters when shear forces cease to exist.

Dilute water that could infiltrate during and after an ice age contains a few mM salts, of which a fraction is calcium ions. In such waters the smectite forms stacks with many tens of smectite sheets that are too heavy to form sol. The stacks can sediment in sloping fractures. Early during the expansion the stacks do not form but after expanding some meters the calcium fraction in the smectite at the interface exceeds 90 % and stacks form. With available information it is an open question whether the slurry of the stacks that builds up at the interface could impede further expansion of clay in the fractures.

It was also found that ion transport in the pores in the rock matrix could considerably limit the expansion under dilute water conditions.

There is considerable evidence that the ten percent or more of non-smectite minerals in bentonite influences the rate of expansion but the mechanisms are not fully understood.

In short: All studied dilute groundwaters contain some calcium. Smectite *equilibrated* with such waters is sufficient to make the smectite fill more than 90 % of the ion exchange positions with calcium. Such smectite cannot form sol. Equilibrium conditions will more readily be reached the further out the clay has expanded into the fracture. Already a few meters clay expansion will ensure that this is attained.

Sammanfattning

I ett KBS-3-typ av förvar kommer vatten som strömmar i sprickor att bära joner till gränsytan mellan sipprande vatten och bentonit som expanderar från deponeringshålet. Vi har studerat hur förhållandena vid leravattengränsytan påverkas av de i den ursprungliga leran och i olika grundvattensammansättningar och av jondiffusionen i lera och mellan grundvatten och leran vid gränsytan.

Vattenflödet, koncentrationen av olika joner vid gränsytan och massöverföringen över gränsytan och i själva leran bestämmer sammansättningen av jonerna i jonbytespositioner i smektiten vid gränssnittet. Detta avgör i sin tur om smektiten kan lösa sig och bilda en sol som kan transporteras bort eller om smektiten kollapsar till mikroskopiska aggregat i sedimentet.

Det finns ett smalt fönster av vattensammansättningar där smektiten kan solubiliseras. Vattnet måste vara utspätt, mindre än cirka 10–30 mM för att detta ska hända (< 0.02 viktprocent salt). Detta är den kritiska koagulationskoncentrationen CCC. I sipprande vatten kan smektitpartiklarna bilda flockar, som kan sedimentera i sluttande sprickor. Flockarna kan åter solubiliseras i stillastående vatten när skjuvkrafter inte längre existerar.

Vatten med låg salthalt som kan infiltrera under och efter istider innehåller några mM-salter, varav en del utgörs av är kalciumjoner. I sådana vatten bildar smektiten aggregat med många tiotals smektitskivor staplade på varandra och är för tunga för att bilda sol. Dessa aggregat kan sedimentera i sluttande sprickor. Tidigt under expansionen bildas inte aggregaten men efter att ha expanderat några meter överstiger kalciumfraktionen i smektiten vid gränsytan 90 % och aggregat bildas. Det är fortfarande en öppen fråga om uppslamningen av aggregaten som byggs upp vid gränsytan kan hindra ytterligare expansion av lera ut i sprickorna.

Det visas också att jontransport i porerna i bergmatrisen avsevärt kan begränsa expansionen under utspädda vattenförhållanden.

Det finns betydande indikationer för att de ca tio procenten eller mer av icke-smektitmineral i bentonit påverkar expansionstakten men mekanismerna är inte helt klarlagda.

Kort sagt: Allt studerat utspätt grundvatten innehåller lite kalcium. Smektit som är i jämvikt med sådant vatten är tillräcklig för att få smektiten att fylla mer än 90 % av jonbytespositioner med kalcium. Sådan smektit kan inte bilda sol. Jonbytesjämvikt kommer lättare att nås ju längre ut leran har expanderat ut i sprickan. Redan några meter leraxpansion torde säkerställa att detta uppnås.

Contents

1 Introduction and background

In the Swedish deep geologic repository for spent nuclear fuel that is planned to be built at Forsmark north of Stockholm the copper canisters with the spent fuel will be surrounded by compacted bentonite clay. When water saturates the clay, this swells and fills out all voids between canister and the walls of the deposition holes. Water seeps in the narrow fractures of the sparse fracture network in the crystalline rock even at repository depth, around 500 m.

Bentonite protects the canister from rock movements. Bentonite is porous and allows ions and solutes to slowly diffuse through it but does not allow water to flow. Bentonite acts as an ion exchanger and retards cationic radionuclide escape, if the canister should be damaged or degraded. In every deposition hole there is tens of tonnes bentonite. It consists of mostly smectite clay but contains also 10 % or more other rock minerals with different solubilities.

Smectite has some interesting and important properties. The smectite crystals form sheets about 1 nm thick and about 300 nm in the other directions. These have permanent negative charges, which are exactly compensated by cations, mostly sodium and calcium. When water enters between the sheets very large swelling pressure results. Should a fracture with seeping water intersect the deposition hole the smectite can swell into the fracture. In low ionic strength water, especially if they are very rich in sodium the smectite particles can form a stable sol, which can carry away the smectite. If large amounts of clay are lost the swelling pressure could decrease and the protective properties could be lost.

In the last decades a number of experimental and theoretical studies have reported many aspects of clay properties and swelling mechanisms, rheologic properties, ion exchange properties and processes that influence the possible loss of smectite into seeping water.

The present report addresses specifically the ion exchange in the smectite clay near the interface between the clay that expands into the fracture and the seeping water. It is at this interface that solubilisation could occur. The potential solubilisation is determined by the water chemistry at the interface. The chemistry at the interface is determined by the composition of the seeping groundwater, the composition of bentonite in the deposition hole, the ion exchange properties and capacity of the clay and the transport mechanisms and rates in the clay and in the seeping water.

1.1 Aims and scope

The main aim is to study and model the ion transport in bentonite clay as used in the KBS-3 repository design and how groundwater and clay composition and ion transport in clay and between clay and groundwater influences the swelling of the clay into fractures and the loss of clay from the deposition holes.

We also aim at exploring some aspects of flocculation of smectite sol that seem to influence the clay loss under some conditions.

2 Bentonite properties

Bentonites contain large amounts of the clay mineral Montmorillonite, which belongs to the Smectite group. Different bentonites also contain varying amounts of other rock forming minerals. Smectite is a sheet mineral forming extremely thin sheets of a layer of aluminium oxide sandwiched between two layers of silicon oxide. The layers form chemical bonds by aluminium and silicon having a bond to the same oxygen atom. The sheet is only one nm thick and several hundred nm in the other directions. Some Al-atoms are substituted by Mg or Fe(II) and some Si in the outer layers are substituted for Al. Because of the substitution the mineral has a deficit of positive charge. This is compensated fully by cations, mainly sodium and calcium that are attached to the outer surfaces of the sheets. When the mineral is wetted by water these cations dissolve in the water but stay very close to the surface in what is called the diffuse double layer, DDL. This can be very thin, a few nm, if the water contains much dissolved ions but can extend to many tens of nm or more in low salinity waters. Two sheets close to each other will have overlapping DDL's, which causes more water to want to be drawn in between the sheets to dilute the very high ion concentration there. This osmotic pressure tries to force the sheets apart. In a confined space this gives rise to very large pressures, up 10 MPa and more, (hundreds of atmospheres) in compressed bentonites. The high swelling pressure will allow the smectite to expand into pores and fractures that are large enough to allow them to enter. In the same way as any other molecules they move randomly by Brownian motion, also bouncing against the walls.

The other minerals in bentonite have no or negligibly small fixed charges. Their size ranges from that of the smectite particles up to a small fraction of a mm. They are pushed along by expanding smectite as the bentonite expands.

2.1 Our conceptual picture of smectite clays and bentonites

This section is essentially a verbatim reproduction of a section in Neretnieks et al. (2009) and is presented here to convey some of the complexities of the material and to convey some of the unknowns and problems we have to address when modelling bentonite expansion and colloid formation.

The individual smectite stacks are shaped as irregular cards or coins and their size varies. The individual smectite sheets are about 1 nm thick and range in size from some tens of nm to several hundred nm. They are sometimes described as ellipsoidal sheets or platelets. Cadene et al. (2005) investigated size, morphology, and apparent charge of individual Sodium-montmorillonite particles of natural MX-80 sodium montmorillonite with atomic force microscopy (AFM) and photo-correlation spectroscopy (PCS). They found two clay populations with a large variation of length distribution. It may be noted that the AFM measured particle thickness finds a small fraction of particles less than 1 nm thick, even down to 0.6 to 0.8 nm in thickness. Montmorillonite sheets seem to be slightly crumpled. This suggests that there are broken fragments of the sheets present. This may have an impact on the stack properties. Some of the smaller particles were found superimposed onto sheets of the larger, mainly on their borders, presumably indicating a difference in the density of charge. They also found that thickness of tactoids (stacks), increased by sheet stacking, but still remains negligible in comparison to their major length. At higher particle concentration the stacks form aggregates.

At high solid volume fractions, the sheets need to be arranged in stacks (tactoids, aggregates, quasi-crystals and also other names are found in the literature) with many sheets parallel. Figure 2-1 shows an example of an arrangement that could lead to volume fraction of solids of 50 % or more.

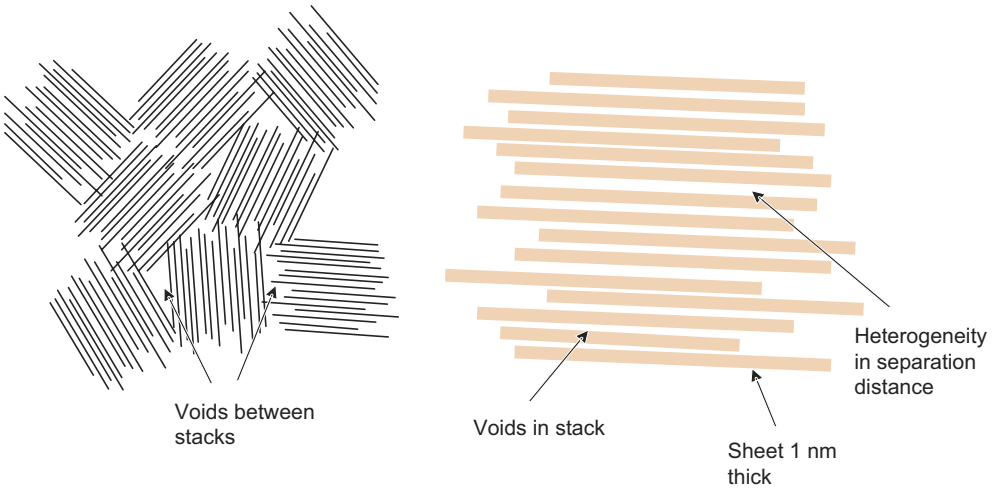

Figure 2-1. *The figure shows how the individual sheets can be arranged in stacks, right hand figure, and how such stacks can be arranged in a compacted system, left figure.*

The individual sheets in the stack are about 1 nm thick. They are somewhat flexible. At a void fraction of 50 % they have approximately the same average distance between the sheets as the sheets are thick. The sheets vary in size and the stacks could be arranged as shown in the left part of Figure 2-1. There will be voids between the stacks that add voids of the system, decreasing the volume fraction of solids further. At higher compactions the distance between the sheets must be less than 1 nm. Charge compensating ions are located between the sheets, which have charge dislocations because of isomorphic substitution of aluminium atoms for magnesium or ferrous iron atoms in the middle octahedral layer formed by an aluminium oxide lattice. This lattice is sandwiched between the two tetrahedral layers of silicon oxide lattice. Typical charge compensating ions are monovalent sodium and divalent calcium ions but also potassium and magnesium ions are found.

When the clay is exposed to water vapour or liquid water the water molecules intrude between the sheets, sorb water on their surface and hydrate the charge compensating ions. This leads to very strong swelling of the clay. Highly compacted bentonite clay with a solid volume fraction $f = 0.7$ (dry density 1 810 kg/m^3) can exert swelling pressures of ten MPa or more when fully water saturated (Karnland et al. 2003, 2006, Pusch and Yong 2006). In low ionic strength waters, the repulsion forces between the sheets can dominate over attractive forces and the particles can disengage from the stacks in the gel and form a stable colloidal sol if given enough water. When sodium is the dominating counterion the particles consist of one or a few sheets (Cadene et al. 2005). When divalent calcium or magnesium dominates the particles or stacks consist of typically 5 to 15 sheets or more (van Olphen 1977, Push and Yong 2006, Bergaya et al. 2006).

Bergaya et al. (2006, Figure 5) show that sodium clay particles with up to 30 to 40 % calcium consist of one to 1.5 sheets on average. With 100 % calcium, stacks with on the average 7 sheets are formed. There can be several reasons for such behaviour. There may be different surface charge densities in different sheets so that attractive and repulsive forces differ between them. This could give rise to separation between parts of the stack during swelling but still retain stacks of several sheets at close distance, potentially caused by the attractive ion-ion correlation effects in the presence of divalent ions on highly charged particles.

Jönsson et al. (2009) predict that smectites with calcium as counterions, even at fairly low calcium fractions, should stop swelling and actually develop strongly cohesive forces between the smectite sheets when the distance between sheets is about 1 nm. This corresponds to a porosity of about 50 % as the sheet thickness is about 1 nm. Simulations show that these attractive forces are very strong at distances shorter than one nm and can dominate over the repulsive double layer forces. At larger sheet distances the repulsive forces dominate even for divalent counterions (Kjellander and Marcelja 1988, Evans and Wennerström 1999, Jönsson et al. 2009). The net force as a function of distance for a calcium smectite is illustrated in Figure 4-2 in Jönsson et al. (2009). A negative osmotic pressure P_{osm}/RT of nearly −1 corresponds to a cohesion pressure of more than 2 MPa. This is a very strong

cohesion pressure. These results suggest that the sheets should collapse into an essentially solid body with sheet distances near 1 nm. Such a body would have a porosity of about 50 %. The body would have a tensile strength comparable to or larger than concrete. This is not observed although stacks with such sheet distances are observed (Pusch and Yong 2006, Bergaya et al. 2006, Birgersson et al. 2009, Jönsson et al. 2009). It is surprising that the stacks repel each other.

Bentonite clays contain a large fraction of smectite but also various amounts of other minerals that are non-swelling. These mineral grains are larger, up to much larger, than the smectite sheets. The solubility of these minerals varies considerably. When bentonite is water saturated, some of the minerals supply the pore water with anions such as chloride, sulphate and carbonate and a corresponding amount of cations. In compacted bentonite, the largest amount of cations are bound to the negatively charged smectite sheets.

2.2 Bentonite swelling and sol formation

2.2.1 Swelling or dilution

As long as there are repulsive forces the clay will try to swell. The swelling rate depends on the balance between the repulsive force(s) and the restraining force caused by the friction between the smectite particles and water. In the swelling clay an identical volume of incoming water will replace the location vacated by the smectite particle. The process is actually a dilution of the clay. In sodium dominated water the swelling would go on forever. When the smectite volume fraction becomes very low the DDL forces become negligible but the particles continue to disperse by the thermally induced random movement of the particles, the Brownian diffusion. The particles form a stable sol.

At higher ionic strengths the repulsive DDL force extend only a short distance and attractive van der Waals forces can overcome the repulsive force and expansion stops. The smectite-water mixture becomes a coherent stable gel that resists tension as well as compression. When water contains much divalent ions such as those of calcium, individual sheets collect in stacks in which the sheets are held very strongly together. The stacks contain tens of sheets at nm distance from each other with water between them. The stack with water has a mass that is many tens of times larger than individual sheet. The stacks repel each other and even this collapsed system swells. However, swelling stops at a volume fraction around 0.05 in the calcium dominated clay, see e.g. Birgersson et al. (2009).

2.2.2 Conditions for sol formation

Birgersson et al. (2009) present two different conditions for when colloids are not expected to be released from swelling clay. One is when the porewater salinity in the clay is larger than the critical coagulation concentration, CCC, which is around several tens of mM, colloids are not released. This is supported on theoretical grounds, see Liu (2010, 2013), Liu et al. (2009 a,b), Birgersson et al. (2011), Wang et al. (2011) and Yang et al. (2017). Another condition is that when the charge fraction of calcium in the smectite is larger than 0.9 the clay forms cohesive stacks of sheets, grains that are only repulsive up to a volume fraction around 0.05 and are too heavy to form colloids and to turn to sol. In its performance assessment, SKB uses a safety function indicator $\sum c_i \times z_i > 4$ mM where c_i is concentration of cations and z_i the charge of the cation (SKB 2010).

During the hundreds of thousands of years of interest, the water composition will change. During and after an ice age, large amounts of melt-water will penetrate to repository depth. During temperate or dry periods, salt from brines at larger depths diffuses upward.

During the temperate period the safety criterion in reference to the summation of the cationic species $\sum c_i \times z_i$ remains much larger than 4 mM. During the glacial cycle, (1) infiltration of dilute glacial melt waters, (2) up-moving of deep saline waters, and (3) the hydrological and the geochemical effects of a frozen soil under the ice sheet, have a strong influence controlling the hydrogeochemical evolution within the candidate repository volume. The calculated safety function is lower than 4 mM in a wide period of the glacial cycle (SKB 2010).

Figure 2-2 shows the range of calcium and sodium concentrations where smectite can form colloids. It is well supported by experiments (Birgersson et al. 2009).

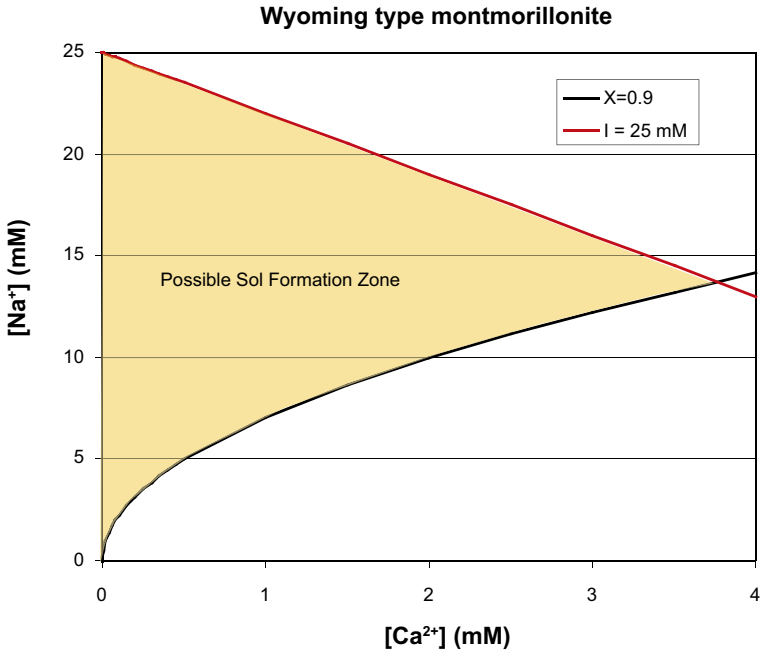

Figure 2-2. *Possible sol formation zone for Wyoming type montmorillonite in equilibrium with external concentrations of $CaCl_2$ and NaCl: the lower limit represents montmorillonite with a 90 % calcium fraction (X) and the upper limit represents a solution ionic strength (I) of 25 mM (from Birgersson et al. 2009).*

2.2.3 Ion exchange equilibria in montmorillonite

The fixed negative charges of smectite particles are always compensated by cations located at the smectite surface when dry and in a close proximity to the surface when immersed in water. Divalent ions such as Ca^{2+} and Mg^{2+} are much more strongly bound than monovalent ions such as Na^{+} and K^{+}. This implies that even a small fraction of divalent ions in the water will result in a large fraction of the divalent cations compensating the smectite charge. It was noted earlier that when more than 90 % of the smectite charge is compensated by Mg and Ca the smectite will not solubilise but form stacks with many tens of sheets with a thin layer of water between the sheets. We will study under what conditions this may occur and how this will influence expansion of the clay.

The above-mentioned ions in the water near to the smectite surfaces are mostly bound by coulombic forces and are not attached to a specific location on the surface but reside in a "diffuse" layer near the surface. These ions are mobile and diffuse in all directions, also along the surface, but on the average always compensate the smectite charges. The "thickness" of the layer can be very thin, on the order of nm, when the bulk water has high concentration of ions but can extend to many tens of nm in very dilute water. See e.g., results of molecular dynamic simulations (Tinnacher et al. 2016, Yang et al. 2017).

The law of mass action for the exchange of ions between bulk water and the fixed charges of ion exchanger states that there will be an equilibrium between the ions in solution and those on ion-exchanger. For the following reaction

$$Ca^{2+} + 2NaX \leftrightarrow 2Na^{+} + CaX_2 \qquad (2\text{-}1)$$

the equilibrium constant for the reaction according to the Gaines-Thomas convention

is written

$$K_{CaNa} = \frac{(Na^{+})^2[CaX_2]}{(Ca^{2+})\,[NaX]^2} \qquad (2\text{-}2)$$

(Na^{+})denotes ion concentration in the water, in this case by sodium. $[CaX_2]$ denotes the equivalent fraction of calcium in the exchanger.

Birgersson et al. (2009) cite experimental values of K_{CaNa} of 2 600 and 4 500 mM for two different smectites. These values are supported by theoretically derived values using the Poisson-Boltzmann theory of 3 200 to 5 300 mM for low and high compacted smectite respectively. There is considerable uncertainty in the values of K_{CaNa} (Idiart et al. 2019).

Besides Ca and Na also the less abundant divalent Mg and the monovalent K have been considered because there are often K-Feldspars and magnesium minerals present both in bentonite clays and in granitic rock. These minerals can release Mg and K to the water. The equilibrium constants for CaNa and MgNa differ by about a factor of two, as do those for CaK and MgK. This can be seen from the data given in the PhreeqC.dat database (Parkhurst and Appelo 1999). They use a different approach to define equilibria for ion exchange but their data can directly be transformed to obtain K_{CaNa} (Bourg and Sposito 2011). The PhreeqC data give somewhat larger values that what is used in this report. It is therefore possible to use the sum of Na and K ions for the monovalent ions and the sum of Ca and Mg concentrations for the divalent ions in the equilibrium equation. We need to account for only one equilibrium constant in this way.

Figure 2-3 shows that when the ion concentration in the water in contact with smectite is low, upper curve, the Ca fraction in the clay will be very close to 1 even when the Ca fraction in the water is very low. This is an important observation in the case of infiltrating dilute waters. These typically contain on the order of totally a sum of a few mM of dissolved salts, see Table 2-1.

As an example, we are going to model a case in which there is compacted clay with a smectite fraction $\phi = 0.5$ in the deposition hole and $\phi = 0.05$ at the interface for different salinities in the porewater that contains only NaCl and $CaCl_2$. Noting that $C_{Na} = C_{An} - 2\,C_{Ca}$, Equation 2-2 also can be written

$$K_{CaNa} = \frac{c_{Na}^2 X_{Ca}}{c_{Ca} X_{Na}^2} = \frac{(c_{An} - 2c_{Ca})^2 X_{Ca}}{c_{Ca}(1 - X_{Ca})^2} \qquad (2\text{-}3)$$

where $C_{An} = \sum c_i \times z_i$ for all anions.

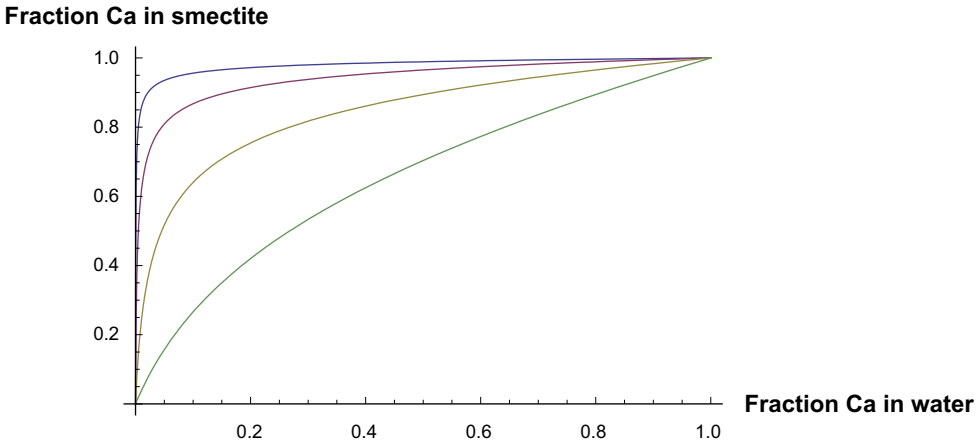

Figure 2-3. *Fraction of calcium in the smectite as a function of the fraction of calcium in the water for four total concentrations in water. 1, 10, 100 and 1.000 mM from left to right, exemplified for K_{CaNa} = 4 000 mM, using Equation (2-2).*

Figure 2-4 shows how a fraction of C_{Ca}/C_{An} changes with C_{An} to attain an equilibrium X_{Ca} of 0.9 and 0.95. It is seen that the smaller the total salinity, concentration C_{An} is, the less Ca is needed to reach a given X_{Ca}. This illustrates that in low salinity water a very small fraction of calcium in the water suffices to reach $X_{Ca} > 0.9$.

Another way to illustrate the impact of ion exchange equilibria on erosion is presented in Figures 2-5 and 2-6. Figure 2-5 shows X_{Ca} when it exceeds 0.9 in the range of concentrations up to 25 mM, which is taken to be CCC for pure sodium ion concentration.

It illustrates that at low concentrations there is a considerable range of combinations of C_{An} and C_{Ca} where erosion is possible. This is a region in which groundwater compositions between dilute and below CCC conditions can be expected over the times of interest, i.e. 10^5 to 10^6 years.

Figure 2-6 shows the same information for the range of observed dilute waters.

It may be noted that SKB's criterion essentially says the same thing as $X_{Ca} > 0.83$. This is shown in Figure 2-7.

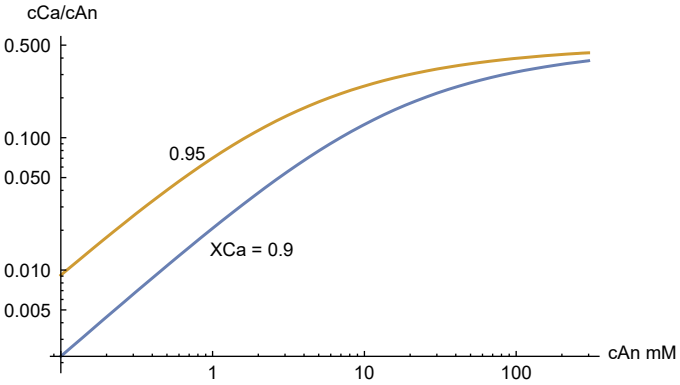

Figure 2-4. *C_{Ca}/C_{An} versus C_{An} for X_{Ca} 0.9 and 0.95.*

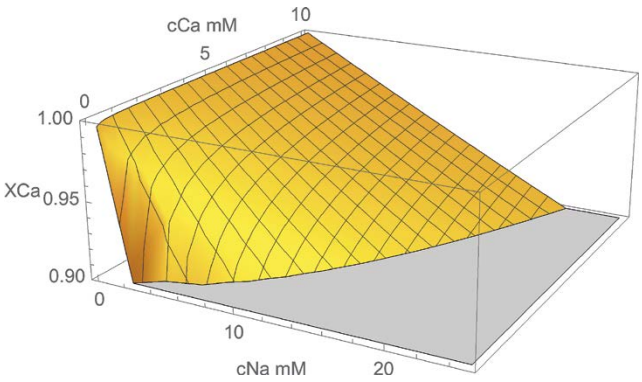

Figure 2-5. *X_{Ca} as function of C_{Na} and C_{Ca} in the range up to C_{Na} =25 mM.*

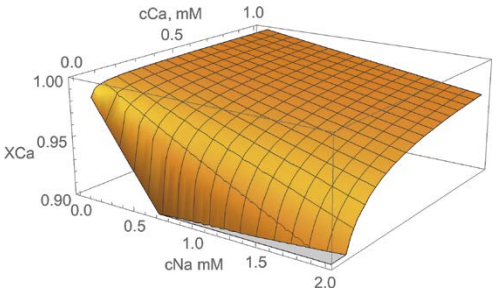

Figure 2-6. *X_{Ca} as function of C_{Na} and C_{Ca} in the range up to C_{Na} =2 mM.*

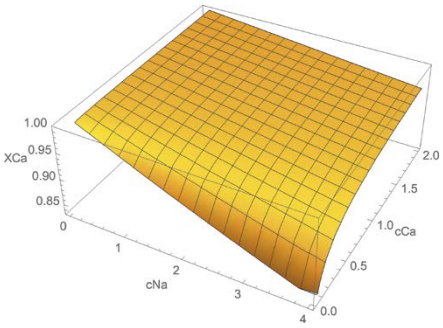

Figure 2-7. *X_{Ca} as function of C_{Na} and C_{Ca} in the range up to C_{Na} = 4 mM. and C_{Ca} = 2 mM.*

Table 2-1 summarises information of different glacial waters and what X_{Ca} would be attained for smectite when equilibrated with them. Neretnieks et al. (2009).

Table 2-1. Data from Brown (2002). The X_{Ca} column shows what the equilibrium fraction of divalent ions should be in ion exchange positions calculated using the sum of monovalent and sum of divalent ions in solution.

	Ca mM	Mg mM	Na mM	K mM	Divalent	Monovalent	X_{Ca}
	0.275	0.018	0.025	0.061	0.293	0.086	0.997
	0.158	0.016	0.0205	0.0117	0.1735	0.0322	0.999
	0.012	0.0023	0.0166	0.0027	0.0140	0.0193	0.997
	0.116	0.0515	0.0258	0.0178	0.1675	0.0436	0.998
	0.380	0.051	0.057	0.0176	0.4305	0.0746	0.998
	0.041	0.0031	0.0225	0.0038	0.0441	0.0263	0.998
	0.604	0.079	0.487	0.056	0.682	0.543	0.990
	0.388	0.156	1.1575	0.0995	0.544	1.257	0.973
	0.213	0.0051	0.0043	0.0027	0.218	0.0071	0.9998
	0.319	0.046	0.0049	0.0063	0.365	0.0112	0.9997
	0.084	0.012	0.045	0.0365	0.0956	0.0815	0.966
	0.105	0.097	0.425	0.0120	0.202	0.437	0.985
	0.121	0.023	0.075	0.005	0.144	0.08	0.997
	0.095	0.033	0.0065	0.0026	0.127	0.0091	0.9996
	0.176	0.017	0.112	0.0135	0.193	0.125	0.996
	0.180	0.058	0.482	0.012	0.237	0.494	0.984
	0.173	0.012	0.076	0.0166	0.185	0.0926	0.997
	0.125	0.018	0.050	0.0056	0.143	0.0551	0.998
Minimum	0.012	0.002	0.004	0.003	0.014	0.007	
Average	0.198	0.039	0.172	0.021	0.237	0.193	
Maximum	0.604	0.156	1.158	0.100	0.683	1.257	
Grimsel meltwater, Missana et al. (2003)							
	0.137	0.0007	0.685	0.0004	0.138	0.685	0.971
Preliminary data proposed for Laxemar 2020 in SR-Can							
	0.38	0.26	2.42	0.06	0.64	2.48	0.952

Evidently, if seeping dilute water could equilibrate with smectite at the interface of the expanding clay it could not release colloids. In the next section it will be explored how transport process in the clay and between interface and seeping groundwater will promote or hinder equilibrium to result.

2.3 Overview of the problem

The clay buffer that surrounds and protects the waste canister allows ions to migrate by molecular diffusion. We start when the clay has been fully water saturated and equilibrated and when the ion exchange sites have been equilibrated with the ions in the pore water. The ion concentrations in the porewater and the composition of the smectite sites are then known. In the compacted bentonite with a porosity around 0.5, by far most of the cations are bound to the smectite, compensating the fixed negative charges in it. Most of the cations on the smectite are bound by the electrostatic forces, and are mobile. Some cations are also bound by surface complexation. The latter are much less mobile and we neglect their mobility in the present study, considering only sodium, potassium, calcium and magnesium.

Consider the following scenario. Some smectite has expanded out into a narrow fracture in which water is seeping. The expansion has reached a certain distance Δr. At the interface the fraction of divalent ions Ca^{2+} and Mg^{2+} on the smectite has occupied 90 % of the sites and the smectite paste ceases to release smectite particle as sol. The smectite particles form coherent stacks that contain up to many tens of individual smectite sheets. These stacks, some 200–300 nm large, although slightly repulsive against each other cannot solubilise and they sediment in the fracture. They must be pushed by the expanding smectite behind them for further expansion of the clay to take place. It is like pushing a fine sand into a fracture. The rheologic properties of the suspension of these grains will influence how this suspension is pushed further out in the fracture.

We wish to study under which conditions this scenario may be valid. Below we describe the main chemical, physical and transport processes involved that influence the formation of stacks.

Figure 2-8 illustrates ion transport in clay that has expanded into a fracture from the deposition hole. The concentration in the free pore water c is higher than in the seeping dilute groundwater c_{GW} and the ions will diffuse towards the clay-water interface. Although the total concentration in the GW is very low the high preference for calcium in X-phase is large, cf. Figure 2-3, favours large X_{Ca} fractions. The rate of transport of Ca from the dilute GW given by the equivalent flowrate Q_{eq} compared to the rate of supply of Na from the deposition hole, DH, given by diffusion in the X-phase as well as in the free water in the pores will determine the water composition at the clay water interface and the X_{Ca}.

This is quantified by the modelling in Chapter 3.

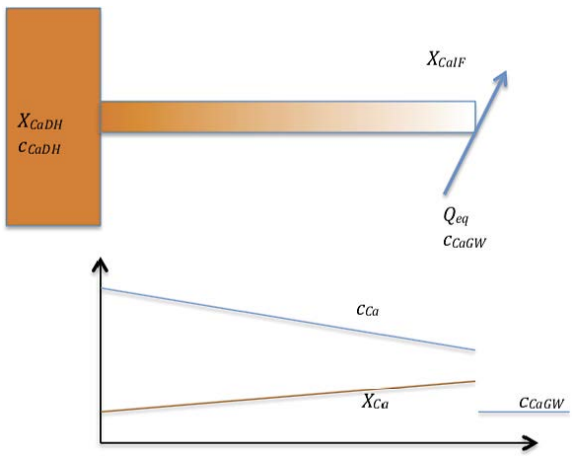

Figure 2-8. *Illustration of concentration of calcium ions in pore water and in ion exchange positions X_{Ca} of calcium in clay in a fracture. In the pore water Ca transport is towards the interface whereas it is in the other direction in the X-phase.*

3 Ion transport in bentonite

3.1 Modelling ion transport

3.1.1 Two concepts

In one concept the clay is considered to consist of two phases, the *free water* and the X-phase, a homogeneous nano-porous material with fixed negative charges evenly distributed in it. The volume fraction of free water is expressed as volume of free water / total water volume.

The negative charges are fully compensated by cations. The cations are mobile and can diffuse in the X-phase. In the free water anions as well as an equal amount of cation equivalents can diffuse (Alt-Epping et al. 2018, Bourg et al. 2003, 2018, Molera and Eriksen 2002, Glaus et al. 2015, 2020, Idiart and Pękala 2016, Kozaki et al. 2005, Sato et al. 1992, Tinnacher et al. 2016, Tournassat and Appelo 2011, Van Loon et al. 2007).

A wide variety of such ion exchanger materials have long been used in industry and laboratory in various applications, to change the ion composition of water and even to de-ionise water. Then both cation and anion exchangers are used. In the anion-exchanger the fixed charges are positive. The commercial ion exchangers are manufactured as small plastic pellets or as thin plastic sheets. A common use is to fill columns with the pellets through which water is passed. In the column there exist two phases, the *free water* and the X-phase, the pellets with the fixed charges. This is very similar to the conditions in the clay, in which the smectite sheets hold the negative charge and make up the ion exchanger, the X-phase. The material in this conceptualisation consists of the *free water* and the X-phase, which also contains water between the sheets as illustrated in Figure 2-1.

In the other conceptualisation, the Donnan model the ion exchanger is conceived as a gel that contains no free water. It forms an integral part of the gel. Anions may enter into the gel. The larger the anion concentration is in the water in contact with the gel the more anions can enter it. The larger the density (concentration) of the fixed charges there is in the gel the less anions can enter. The anions are said to be excluded from the gel to a certain degree. This is called an exclusion factor and gives the ratio of anion concentration in the gel to that in the free water outside. It is derived from the Donnan equilibrium concept (Birgersson and Karnland 2009, Gimmi and Alt-Epping 2018).

The diffusion properties of ions in the gel can be determined by experiments and the flux of ions through the gel will be proportional to the concentration difference over it. Because of the anion exclusion the cation flux will be much larger than anion flux for a given concentration difference in the water on both sides of the gel.

The ion transport through clay can be modelled in two ways. In the pure Donnan approach the clay contains no free water and the diffusion is modelled as Fickian diffusion accounting for the ion exclusion effect for the anions. The other way is to model it as parallel diffusion in free water for the both an- and cations and diffusion in the X-phase of cations only. It is assumed that everywhere there is equilibrium between the concentrations in free water and X-phase. The volume fraction of free water is then assumed to be on the order of the exclusion factor.

We use the “free water” approach for several reasons. One is that it seems more realistic to assume that there is actually some connected free water between the stacks of sheets, see Figure 2-1, and that there are non-swelling non-charged minerals present in bentonite clay that also have a thin layer of water around them. The ion transport in bentonite can then be considered to be like in a “leaking” Donnan gel.

3.1.2 Ion transport in clay – free water model

In the expanding stacks of smectite sheets in the compacted bentonite, the water in the narrow space between the sheets contains all the cations that compensate the fixed negative charges in the sheets. No anions can enter there. Between the irregular stacks the water is more distant from the sheet surfaces and anions are less repelled and can enter there. Also, the irregularities between the stacks and around

the very fine sand particles that make up on the order of tens of percent of bentonite contain free water. In the free water anions and an equal amount of cations, by charge balance, exist. The ions in the *free water* and the X-phase are in equilibrium locally everywhere.

In a column or slot (fracture) filled with clay, ions will diffuse through the clay in the slot when its two ends are subjected to waters with different concentrations. The ion flux through the slot will take place both in the *free water* and in the X-phase. The flux J_i of ion *"i"* is described by the diffusion equation

$$J_i = -D_q\phi\ \frac{dq_i}{dr} - D_{FW}(1-\phi)\frac{dc_i}{dr} \tag{3-1}$$

D_q is diffusion coefficient in the X-phase, D_{FW} that in the *free water*. q_i is concentration in the X-phase and c_i that in the water. ϕ is the volume fraction of clay in the slot and $(1-\phi)$ is the volume fraction of *free water*. In analogy to definition of pore diffusivity D_p that accounts for constrictivity δ_{Constr} and tortuosity τ^2 of the pores we define D_{FW} using Archie's "law" to estimate the effects of these entities.

$$D_{FW} = \frac{D_w\delta_{Constr}}{\tau^2} = D_w(1-\phi)^{0.6} \tag{3-2}$$

Considering that equilibrium between the two phases, either q_i or c_i can be eliminated in Equation 3-1 and the equation can be written

$$J_i = -D_q\phi\ \frac{dq_i}{dc_i}\frac{dc_i}{dr} - D_{FW}(1-\phi)\frac{dc_i}{dr} \tag{3-3a}$$

or

$$J_i = -D_q\phi\ \frac{dq_i}{dr} - D_{FW}(1-\phi)\frac{dc_i}{dq_i}\frac{dq_i}{dr} \tag{3-3b}$$

$\frac{dq_i}{dc_i}$ is determined from the ion exchange equilibrium equation Equation (2-3).

It should be noted that the same ion can diffuse in one direction in the X-phase and in the opposite direction in the free water in the same location. $\frac{dq_i}{dc_i}$ varies considerably with concentration and thus also with location in the slit. We note also that for anions Equation (3-1) reduces to

$$J_{i,An} = -D_{FW}(1-\phi)\frac{dc_{i,An}}{dr} \tag{3-4}$$

The anion transport in the free pore water is accompanied by the transport of an identical amount of equivalents of cations. In addition to the cations in the free water there are cations in the interlayers between the smectite sheets. The system is idealised by assuming that the water between the smectite sheets in stacks only contains cations in an amount that exactly compensates the amount of negative charges in the sheets.

The flux of cation "i" in the free water is

$$J_{i,FW} = J_{An,tot}\frac{c_i}{c_{An,tot}} \tag{3-5}$$

The ions in the X-sites diffuse with a rate proportional to the concentration gradient $\frac{dq_i}{dr}$ in the ion exchange sites.

q_i is the concentration in the X-phase

$$q_i = X_i\ CEC\ \rho_s \tag{3-6}$$

$$J_{i,X} = -D_q\phi\ CEC\ \rho_s\frac{dX_i}{dr} = -D_X\frac{dX_i}{dr} \tag{3-7}$$

Equation 3-7 also defines $D_X = D_q\phi\ CEC\ \rho_s$

The cation flux ion in free water and in X can now be written

$$J_{i,tot} = J_{An,tot}\frac{c_i}{c_{An,tot}} - D_X\frac{dX_i}{dr} \tag{3-8}$$

3.1.3 Transport between clay-water interface and seeping water

Figure 3-1 illustrates clay that has expanded from the deposition hole into a fracture and how water seeps past the clay. A solute diffuses from the interface into the seeping water. The mass transfer rate between the clay water interface and the seeping water is proportional to the concentration difference at the interface, $c_{i,IF}$, and the concentration in the approaching seeping water $c_{i,GW}$. The transfer rate also depends on how fast the solute species concentration in the seeping water builds up by molecular diffusion during the time water is in contact with the clay.

Solving the flow and diffusion equations for flow around the cylindrical clay/water interface gives a very simple relation (Neretnieks et al. 2010). The rate of transport of ion "i", N_i, from interface to water is

$$N_i = Q_{eq}\,(c_{i,IF} - c_{i,GW}) \tag{3-9}$$

$c_{i,IF}$ is the concentration at the interface, $c_{i,GW}$ that in the approaching water, δ is the fracture aperture, D_w is the diffusion coefficient in water of the species, r_{IF} the is radius of the circular interface and u_w *is* the water velocity in the fracture.

$$Q_{eq} = 4.51\,\delta\sqrt{D_w r_{IF}\,u_w} \tag{3-10}$$

This is convenient because Q_{eq} is practically the same for all small molecules and ions because D_w very little depends on the diffusing species. The equivalent flowrate Q_{eq} is introduced here because it is used in the modelling of both clay erosion and radionuclide transport in performance assessment calculations and is a useful entity in performance measure.

It may also be noted that in sloping fractures the water can be mobilised by the diffusion of salts between the clay and water in the fracture as this generates buoyancy induced flow. The flow can be downward or upward depending of if the GW at the IF becomes denser or less dense by the salt diffusion (Neretnieks and Winberg-Wang 2019). There thus need not be a hydraulic gradient to generate flow.

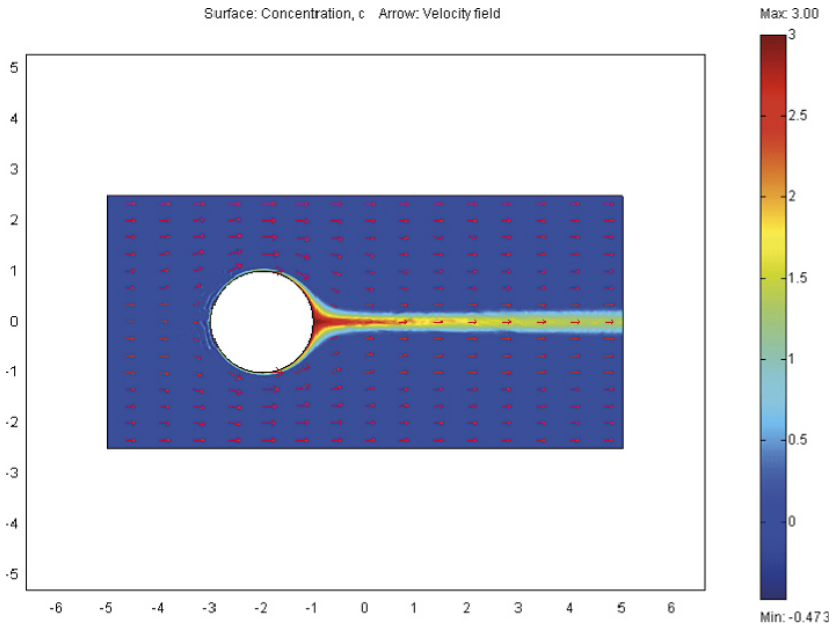

Figure 3-1. *Groundwater flows in the intersecting fracture around the clay that has expanded out from the deposition hole. A solute diffuses into the passing groundwater. The concentration is shown by the colour surface plot and the groundwater velocity by the arrow plot (Moreno et al. 2011).*

For the anion the transport rate through bentonite in the fracture at steady state is the same and can be denoted by

$$N_{An,i} = -D_{FW}\varepsilon_{FW}(1-\phi)A_{slit}\frac{dc_{An,i}}{dr} \quad (3\text{-}11)$$

$$A_{slit} = 2\pi r\delta \quad (3\text{-}12)$$

The clay has expanded into the fracture by a diffusion-like process with a near constant diffusivity (Liu 2010). The volume fraction ϕ of clay in the fracture decreases from the radius of the deposition hole r_{DH} to the radius of the expanded clay $r_{IF} = r_{DH} + \Delta r$.

The transport rate $N_{An,i}$ of the anion in the clay is equal to the rate at which it is transported to or from the interface by the seeping water and combining the two expressions Equation 3-9 and 3-11 gives

$$-D_{FW}\varepsilon_{FW}(1-\phi)A_{slit}\frac{dc_{An,i}}{dr} = Q_{eq}\left(c_{An,i,IF} - c_{An,i,GW}\right) \quad (3\text{-}13)$$

At steady state the anion concentration profile for radial diffusion is

$$c_{An,i}(r) = c_{An,i}(r_{DH}) - \left(c_{An,i}(r_{DH}) - c_{An,i}(r_{IF})\right)\frac{\ln(r/r_{DH})}{\ln(r_{IF}/r_{DH})} \quad (3\text{-}14)$$

The boundary condition at the inner boundary $r = r_{DH}$ where the fracture is in contact with the large volume of compacted bentonite is taken to be the "known" pore water anion concentration in the mass of bentonite buffer $c_{An,DH}$.

The above two equations suffice to determine $c_{An,i,IF}$ and then the anion concentration profile in the free water is given. However, the concentration of the cations in the free water depends on how these interact with the cation fraction X_i in the X-phase via the equilibrium relation Equation 2-3.

Utilising the solution for the anion transport, the total transport rate for cation "i" in the free water as well as that in the X-phase can be written

$$N_{i,tot} = A_{slit}J_{i,tot} = N_{An,tot}\frac{c_i}{c_{An,tot}} - D_q\phi\, A_{slit}\frac{dq_i}{dr} = Q_{eq}\left(c_{An,i,IF} - c_{An,i,GW}\right) \quad (3\text{-}15)$$

With Equation 3-7 this gives

$$N_{An,tot}\frac{c_i}{c_{An,tot}} - D_X A_{slit}\frac{dX_i}{dr} = Q_{eq}\left(c_{i,IF} - c_{i,GW}\right) \quad (3\text{-}16)$$

At the rim $X_{i,IF}$ is in equilibrium with $c_{i,IF}$ and $c_{An,tot,IF}$.

3.2 Solving the equations

We assume that all anion diffusion coefficients are the same and then need not distinguish the different anions. They can be treated as one single entity accounting for the transport of negative charge by the anions $c_{An,tot}$. When the concentration of the anions is known in the source as well as in the groundwater Equation 3-16 coupled to Equation 2-3 can be solved. The solution gives concentration profile of the anion $c_{An,i}$ (r) as well as the concentration at the clay-water interface, $c_{An,tot,IF}$. It also gives the total anion equivalent concentration, profile, $c_{An,tot}$ (r) as the sum of the anions with different charges.

$$c_{An,tot} = \Sigma\, z_i\, c_{An,i} \quad (3\text{-}17)$$

To obtain the fractions X_i and the cation concentrations at the interface r_{IF} for a system with n cations we need to solve n-1 equations Equation 3-16 simultaneously using the knowledge that $\Sigma\, X_i = 1$. For a two-component system it suffices to solve only one equation. In the examples below we consider two cations, calcium and sodium.

Choosing Ca of the two species Ca and Na, the equation to solve then is

$$N_{An,tot}\frac{cCa}{c_{An,tot}} - D_X A_{slit}\frac{dX_{Ca}}{dr} = Q_{eq}\left(c_{Ca,IF} - c_{Ca,GW}\right) \quad (3\text{-}18)$$

As indicated earlier $N_{An,tot}$ and $c_{An,tot}$ do not depend on the cation transport. Equation 3-13 and 3-14 are solved first.

The equilibrium Equation 2-3 gives

$$K_{CaNa} = \frac{c_{Na}^2 X_{Ca}}{c_{Ca} X_{Na}^2} = \frac{(c_{An,tot} - 2c_{Ca,IF})^2 X_{Ca,IF}}{c_{Ca,IF}(1 - X_{Ca,IF})^2} \quad (3\text{-}19)$$

Using Equation 3-19, $c_{Ca,IF}$ is function of only $X_{Ca,IF}$ and $c_{An,tot}$.

As the latter is known from the anion profile, Equation 3-18 is function of only $X_{Ca,IF}$. This can be found by some suitable root-finding numerical routine combined with a solver of an ordinary non-linear differential equation of a boundary value problem. We have used the Mathematica routines "Findroot" and "NDSolve", Wolfram Mathematica 12.1.

3.3 Examples for the steady state and exploration of sensitivity to various data

3.3.1 Data for the central case

Table 3-1 shows data for the central case. The cases are chosen to represent dilute water chemistry as well as near CCC conditions. It is based on the KBS-3 geometry and fairly high fracture transmissivity. The aperture 0.1 mm is chosen to be consistent to the transmissivity $T = 10^{-7}$ m^2/s but is taken to be 2.5 times higher than the cubic law aperture for this transmissivity.

Table 3-1. Parameter values for the central case(s). (z.z) means alternative values including near CCC conditions for sodium rich waters.

$c_{An,GW}$ mM	$c_{Ca,GW}$ mM	$c_{Na,GW}$ mM	$X_{Ca,DH}$ -	$c_{An,DH}$ mM	$c_{Ca,DH}$ mM	$c_{Na,DH}$ mM
1.0 (30)	0.14 (4.5)	0.72 (21.0)	0.3 (0.1, 0.3)	300	60	180

Table 3-1 continued.

T m^2/s	δ mm	grad -	$D_q\phi$ m^2/s	D_w m^2/s	CEC eqv/kg	K_{CaNa} mM	ε_{FW} -
10^{-7} (10^{-8})	0.1	0.03	2×10^{-11}	2×10^{-9}	0.8	4 000	0.01 (0.1)

Comments on the data in Table 3-1.

The Grimsel glacial water was chosen because there are a few experiments using it in expansion tests in artificial fractures. The pore water composition in the DH is based on mineral equilibrium simulations but was chosen much higher to include the possible presence of more soluble minerals e.g. NaCl not accounted for in the PhreeqC simulations (Neretnieks et al. 2009). This choice is conservative as was also found in the sensitivity analysis. Transmissivity of fractures intersecting DH's will be measured and high transmissivity DH's will be discarded. The chosen value is on the high side. The aperture is also on the high side, see appendix in Neretnieks (2019). The aperture as such does not influence the results for solution of the equations discussed except for the magnitude of the rate of ion flowrate *Ni*, which is proportional to the fracture aperture. This is seen in e.g. Equation 3-18 where cross-section for diffusion A_{slit}, N_{An} and the equivalent flowrate Q_{eq} are proportional to the fracture aperture. The hydraulic gradient is chosen in the high end of the expected span. $D_q\phi$ is based on Sato et al. (1992) data for Strontium, which forms a divalent ion with similar chemistry as calcium. It is about ten times larger than the data in for strontium from Molera and Eriksen (2002). Glaus et al. (2015) found considerably larger values for Strontium, around 10^{-9} m^2/s and Glaus et al. (2020) found

several values 10, 30 and 90 times larger than 10^{-9} m^2/s in low ionic strength waters in Illite clay. This is very much larger than diffusion in un-confined water, which is not likely to be correct and casts doubts on the evaluation method used. The experimental methods used by Sato et al. (1992) and the other groups were different, Sato measured the concentration profiles in compacted clay samples in which the source of nuclides had been sandwiched between two compacted clay samples. The other experiments were so-called through diffusion experiments in which the ions diffuse through compacted clay between two filters, from one vessel to another. This difference is one of the main causes of uncertainty. We try to illuminate the problem in simple sensitivity tests.

3.3.2 Dilute water

The simulations below assume that steady state conditions are reached. We will later show that this is a fair assumption. As the clay expands from the DH, the diffusion distance Δr to the interface, IF, increases. Cations in the free water, FW, diffuse from the deposition hole, DH, towards the IF, as also do ions from the GW. The anions diffuse only in the FW from the high concentration in the DH towards the seeping GW. The calcium that has a higher X_{Ca} at the IF than in the DH diffuses towards the DH in the X-phase. This is illustrated in Figure 3-2. The sodium ions diffuse in the other direction in the X-phase.

Figure 3-3 shows $c_{Ca,IF}$ as function of Δr for different $X_{Ca,DH}$. Calcium concentration in water at the IF is rapidly depleted by uptake in the X-phase when the clay has expanded only a small distance. The concentration increases with increasing Δr and approaches $c_{Ca,GW}$ more and more.

The Na concentration at the interface will similarly decrease from that in the GW, c_{NaGW} = 0.72 mM, to 1–2 × $c_{Ca,IF}$.

The flowrate of calcium from the GW in the direction toward the DH was around

$1–2 \times 10^{-11}$ mol /s, $(3–6 \times 10^{-4}$ mol/yr) in the three cases.

Figure 3-4 shows X_{Ca} at the interface as function of Δr.

It is seen that a few meters expansion distance of clay in the fracture suffices for X_{Ca} at the IF to become 0.9 and larger, even when the bentonite in the DH has a small fraction of calcium. The more calcium rich the bentonite in the DH is the smaller will be the expansion to reach X_{Ca} = 0.9.

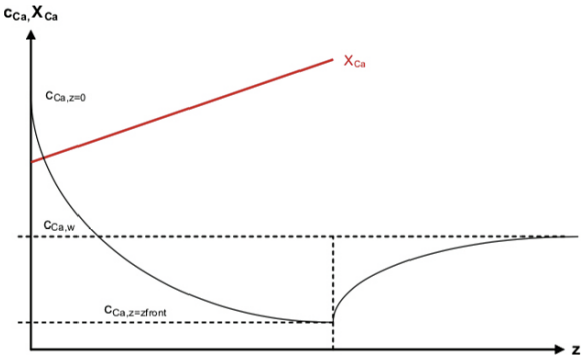

Figure 3-2. *Concentration profiles of calcium in smectite, calcium in free water and in seeping $c_{Ca,w}$ water. Vertical dotted line shows location of interface.*

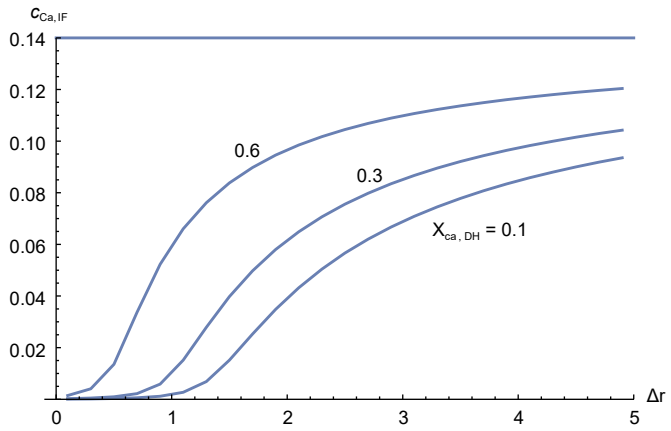

Figure 3-3. *c_{Ca} (mM) at the interface as function of distance to the interface Δr (m) for three different values of X_{Ca} in the deposition hole. The horizontal line shows c_{CaGW}.*

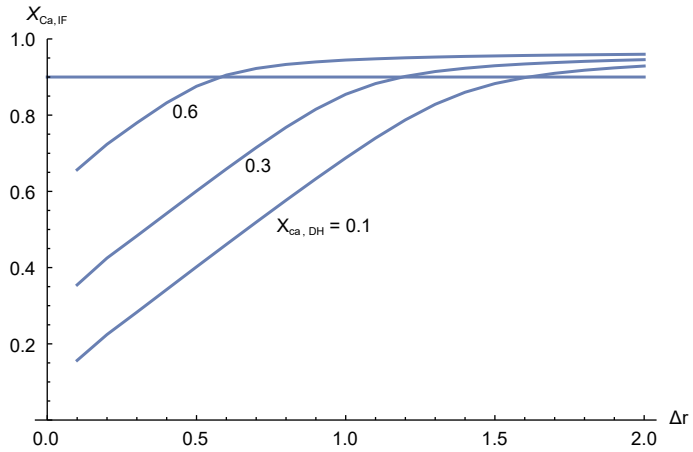

Figure 3-4. *X_{Ca} at the interface as function of distance to the interface Δr (m) for three different values of X_{Ca} in the deposition hole. The horizontal line shows X_{Ca} = 0.9.*

3.3.3 Simple sensitivity estimates to various data

The volume fraction of smectite ϕ in the DH was chosen to be 0.5 and ϕ at the IF was 0.05, which is around the volume fraction at which a calcium-dominated smectite will stop expanding. The steady state expansion is not influenced by ϕ when the product $D_q\phi$ of the diffusion coefficient in the X-phase D_q and the volume fraction is constant, which it has been found to be for monovalent as well as divalent cations (Sato et al. 1992, and Kozaki et al. (2005) as summarized in Neretnieks et al. (2009).

The anion concentration in the free water in the DH has negligible influence on both the c_{Ca} at the IF. Also, the fraction of the water volume in the clay ε_{FW}, when changed from 0.01 to 0.1 has marginal influence. This is because the transport in the free water of Ca and Na is much smaller than that in the X-phase.

Keeping the aperture at 0.1 mm but changing the transmissivity to ten times smaller, i.e. $T = 10^{-8}$ m^2/s the mass transfer rate Q_{eq} between seeping GW and the IF, is lower and the calcium from the GW dissipates faster into the DH. It takes a larger Δr to compensate for this as seen in Figure 3-5.

Figure 3-6 shows X_{Ca} at the interface as function of distance to the interface Δr for three different values of X_{Ca} in the deposition hole for a ten times larger value of $D_q\phi$. The horizontal line shows $X_{Ca} = 0.9$.

The front will expand considerably longer distance to attain $X_{Ca} > 0.9$.

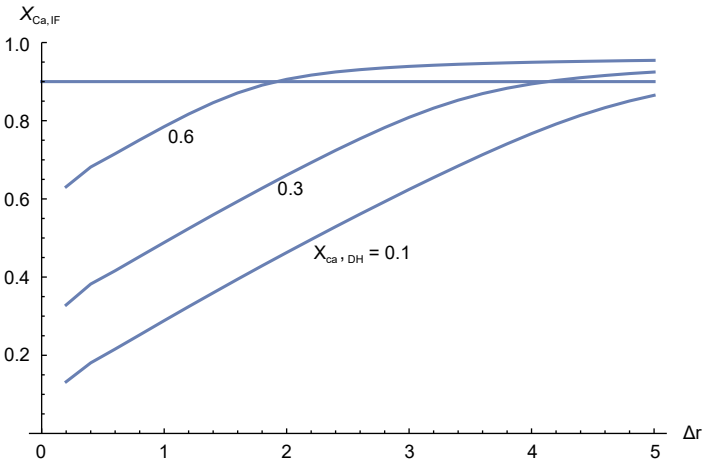

Figure 3-5. *X_{Ca} at the interface as function of distance to the interface Δr (m) for three different values of X_{Ca} in the deposition hole. The horizontal line shows $X_{Ca} = 0.9$.*

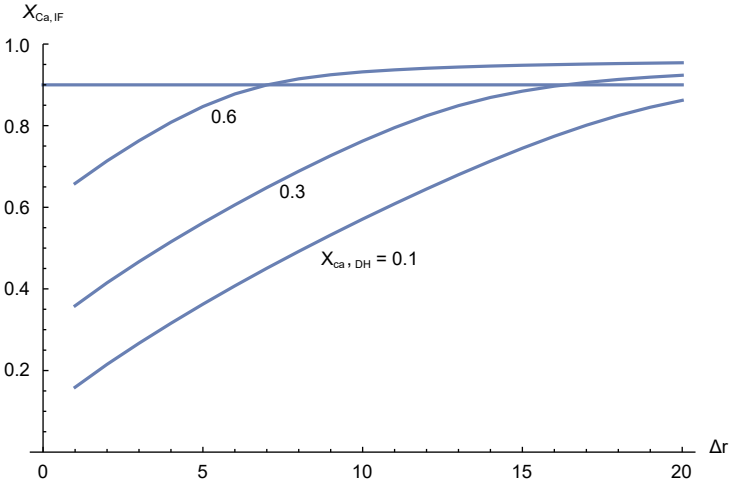

Figure 3-6. *X_{Ca} at the interface as function of distance to the interface Δr (m) for three different values of X_{Ca} in the deposition hole. $D_q\phi = 2 \times 10^{-10}$ m^2/s.*

3.3.4 Discussions and conclusions from the dilute water examples

In all above examples the Ca transport rate is dominated by that in the X-phase. This is because the free water fraction is small and the transport is further impeded by the effect of Archie's law. Under such conditions the transport in the free water of calcium ions from the IF into the DH could be neglected and Equation 3-18 could be reduced to

$$\frac{dX_{Ca}}{dr} CEC\ \rho_s = -\frac{Q_{eq}}{D_q \phi\ A_{slit}} \left(c_{Ca,IF} - c_{Ca,GW}\right) \qquad (3\text{-}20)$$

From this equation one can see how sensitive the system is to changes or uncertainties in Q_{eq}, $D_q\phi$ and CEC. Indirectly also the sensitivity to K_{CaNa} can be assessed. From the ion exchange equilibrium relation $c_{Ca,IF}$ is a function of $X_{Ca,IF}$ at the IF i.e. at $r = r_{IF}$.

It was seen that even bentonites with low calcium will eventually reach $X_{Ca} = 0.9$ when expanding in fractures with dilute waters. It was also found that the transport in the free water is very small compared to that in the X-phase. This implies that the ion exclusion effect is important to account for when modelling how rapidly the large mass of bentonite in the DH takes up or loses dissolved ions.

3.3.5 Present day Forsmark water and saline waters

Present day concentrations are roughly around a few hundred mM Cl, 30 mM Ca plus Mg and 100 mM Na plus K. The concentrations are sinking at present and can be expected be about 2/3 to ½ as large after 7 000 years (Salas et al. 2010).

With the present-day ion concentrations and the data on diffusion coefficient and other data as in Table 3-1 the pore concentration at the IF will be well above 25 mM but not always have $X_{Ca} > 0.9$ as was shown in Figures 2-5 to 2-7. There is only is a narrow range of compositions when none of the criteria will be fulfilled and smectite may form sol and erode. This is also illustrated in the following example in which a relatively dilute GW is used. Figure 3-7 shows the Na profile for three different X_{Ca} in the deposition hole. The GW contains 30 mM salt of which 21 mM is Na.

The Ca fraction in the X-phase at the interface, X_{CaIF} is 0.852, 0.848 and 0.845 for the three different X_{CaDH} in the DH in falling order for Δr 0.2 m.

In this example the CCC criterion is barely attained with the criterion $c_{Na} > 25$ mM but the $X_{Ca} > 0.9$, is not. $c_{Na,GW}$ 30 to 40 mM will suffice better for this criterion. There will thus be a gap between the dilute GW with a few mM and a GW with around 30 mM salt that satisfies none of the criteria. Higher salinities will always satisfy the CCC criterion.

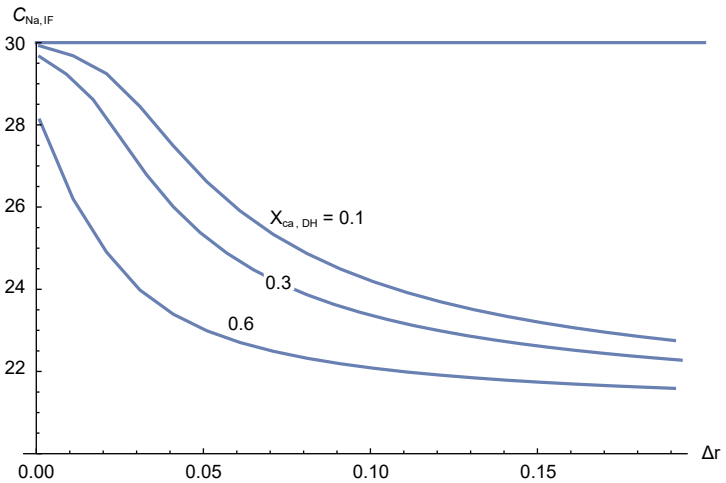

Figure 3-7. *C_{Na}, mM, at the interface as function of distance to the interface Δr (m) for three different values of X_{Ca} in the deposition hole.*

3.4 Evolution of of XCa profile before steady state is attained

In previous section it was assumed that steady state conditions had been established. We want to explore if in the Schatz et al. (2013) and Schatz and Akhanoba (2017) experiments extending over around 1 000 hours and with expansion distances of a few cm such steady may have been attained. The model described below will be used for this purpose but will also be used to see if the steady condition can be expected in PA time scales.

3.4.1 Impact of non-steady state ion exchange

The clay expands driven by DDL forces between the smectite sheets. The expansion can be modelled as diffusion process (Neretnieks et al. 2009). For radial expansion the diffusion equation can be written

$$\frac{\partial \phi}{\partial t} = \frac{1}{r}\frac{\partial}{\partial r}\left(D_{clay} r \frac{\partial \phi}{\partial r}\right) \cong D_{clay}\frac{1}{r}\frac{\partial}{\partial r}\left(r \frac{\partial \phi}{\partial r}\right) \quad (3\text{-}21)$$

D_{clay} depends on ϕ but is on the order of 10^{-10} to 10^{-9} m^2/s in a wide range of volume fractions when ionic strength is above 1 mM of sodium and $X_{Ca} < 0.9$.

In the *free water* model anions will only diffuse in the *free water*. The diffusion in the clay of ions in ion exchange positions, the X-phase dominates or is of the same magnitude as that in the *free water*. This was demonstrated earlier. The instationary diffusion of anions can be described by a similar equation

$$\frac{\partial c_{An}}{\partial t} = \frac{1}{r}\frac{\partial}{\partial r}\left(D_p r \frac{\partial c_{An}}{\partial r}\right) \quad (3\text{-}22)$$

D_p is $D_w \varepsilon_{FW}^{0.6}$ and with $\varepsilon_{FW} = 0.01$, $D_p = 6.1 \times 10^{-11}$ m^2/s.

This implies the anion concentration profile will adapt somewhat slower to that of the evolving ϕ profile change and that consequently the cations in the free water that diffuse from compacted bentonite source in which they have higher concentration than in the low ionic strength seeping groundwater will influence the cation concentration at the IF less.

The instationary diffusion of calcium in the X-phase is described by

$$\frac{\partial(\phi X_{Ca})}{\partial t} = \frac{1}{r}\frac{\partial}{\partial r}\left(\phi D_{Ca} r \frac{\partial X_{Ca}}{\partial r}\right) \cong \phi D_{Ca}\frac{1}{r}\frac{\partial}{\partial r}\left(r \frac{\partial X_{Ca}}{\partial r}\right) \quad (3\text{-}23)$$

This is because ϕD_{Ca} is practically constant as noted earlier and is on the order of 10^{-11} m^2/s. It is thus one to two orders magnitude less than D_{clay}.

The clay expands by soaking up the GW at the IF. As diffusion of ions in the pore water is slower than the expansion of the clay the composition at the IF will be closer to that of the GW than if the concentration profile between IF and DH had been established a steady state. The steady state assumption is thus conservative.

Equation 3-21 has been solved previously under different boundary conditions including cases where there is continuous loss at the rim during expansion (Neretnieks et al. 2009, 2017, Moreno et al. 2010).

The three above Equations 3-21 to 3-23 can be solved simultaneously but at present we do not think that this give any deeper insights considering the input data can vary over considerable ranges and that there is a large number of variables that must be assigned values.

4 Rheology of paste, gel and slurry – impact of salinity and chemical composition

4.1 Overview

A very good paper (Ph.D. Thesis) of the rheology of clays can be found in Pujala (2014).

The water-saturated clay expands as it takes up more water and is diluted. In sodium dominated water the particles can solubilise and be carried away with the seeping water. The sol flows like water although it is somewhat more viscous. It has been found that the sol can form flocs that combine to a gel even when water ionic strength is below CCC. This is caused by the gentle shear force in the parabolic velocity profile in the sol as it flows in the fracture (Neretnieks et al. 2017). The flocs can sediment in sloping fractures, form blobs of gel that stops sedimenting and clog the fracture locally. However, the stagnant gel blob can itself start to solubilize and start the flocculation process again because when the seeping water slows down and stops, parabolic velocity profile induced shear stress stops. The below CCC conditions with sol formation re-establish and sol is formed. This is seen in the experiment displayed in Figure 4-1.

In sloping fractures the rate of smectite loss can be considerably larger than it is in horizontal fractures. It has been speculated that the blobs of gel eventually could fill the fracture, stop water flow and stop or at least slow down further smectite loss. However, the yield strength of the gel is not sufficient to stop the swelling of the paste and the paste will continue to expand approximately as projected in the original assessment (Neretnieks et al. 2009). The possible impact of flocculation on bentonite erosion has been studied by Neretnieks and Moreno (2018).

In above CCC conditions the gel that forms at the interface to the seeping water has yield stress considerably larger than the stress induced by the hydraulic gradient. The paste and gel will not be, but marginally, deformed and will not flow pushed by the seeping water.

In calcium dominated water the paste expands less rapidly because the swelling pressure is smaller. In addition, the paste does not form sol because the individual smectite sheets form stacks of many tens of sheets that are too heavy for sol formation. The paste will not swell beyond about a volume fraction smectite of about 0.05.

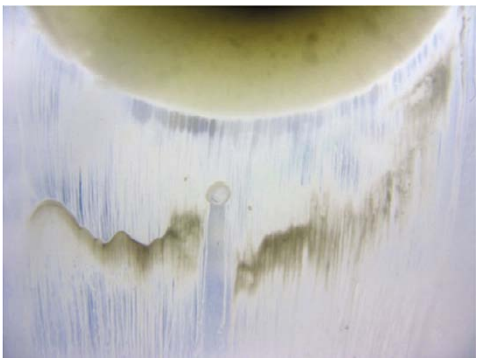

Figure 4-1. *Close-up photographic image of test 9 at 90° rotation from a horizontal fracture position to vertical. From Schatz et al. (2013).*

4.2 Flocculation de-flocculation in below CCC waters

It is well known that shear caused by velocity gradients generate flocculation of smectite particles (Adachi et al. 2019). De-flocculation occurs when shear forces become large enough the overcome the forces that hold the floc together or when chemical conditions change to change the forces and break the bonds. De-flocculation under the conditions of interest here seems not to have been discussed much.

The concept of critical coagulation concentration, CCC, implies that below CCC smectite rapidly forms a stable sol because the repulsive DDL forces are always larger than the attractive vdW forces. Gravity will make the sol denser at the bottom of a vessel than higher up but the individual particles will always repel each other (Neretnieks et al. 2009), This idealised situation is over-simplified. Flocculation of sodium exchanged smectite particles start forming flocs within days in deionised waters and form a gel with distinct yield stress. When agitated, the bonds are broken, sol forms and flocculation starts anew. Below we give our conceptualisation of the processes involved. See Appendix.

Figure 4-1 shows the release and sedimentation of small flocs and that they combine to a large blob that stops sedimenting. We interpret the situation as follows. The individual smecite particles released from the clay water interface sediment slowly. This induces a mild circulation of water. This forces the smectite particles to rotate and bump into each other with edge to face contact. The edges are mildly positive and although there is a spill-over of positive potential from the faces, the edges penetrate this and bind to the faces by coulomb and also by vdW forces. These primary flocs come in contact with each other when larger, more rapidly sedimenting flocs catch up with smaller more slowly sedimenting flocs and combine. The fracture fills with flocs that form a gel. The gel has a yield stress, which is larger than the buoyancy force trying to dislodge it.

However, the now rigid gel is in contact with below CCC water at its lower part and thermal forces (the constant random jittering of the smectite particles) allow release of individual smectite sheets. The sedimentation starts again from the underside of the gel from which the particles sediment once they have been released from the gel.

4.3 Rheology when $X_{Ca} > 0.9$ in the smectite

When $X_{Ca} > 0.9$ at the IF one could hypothesize that this will generate non-swelling stacks of coherent sheets that sediment at the IF, build up a fine sand-like plug that is pushed by the expanding clay behind it. This is like pushing a sand-plug in a narrow slot. This would resist movement by wall friction. One of the experiments in Schatz et al. (2013), Experiment #10 could be interpreted in this way.

We have not found experiments that specifically address the rheology and present data on smectite sediments with $X_{Ca} > 0.9$. Birgersson et al. (2009) studied the rheology swelling of bentonite clays. Attempts to measure strongly calcium dominated smectite suspension were not successful because sediments were rapidly formed. It is hypothesized in the present report that other sediments with very small uncharged alumino-silicates with comparable solid volume fractions may behave similarly and that this may help to understand if $X_{Ca} > 0.9$ smectite can be expected to clog the fracture and prevent further expansion of the clay in the fracture. The range of volume fraction of interest between 0.05 and 0.5.

Sosio and Crosta (2009) measured the rheologic properties of concentrated granular suspensions consisting of varying solid concentration (from 38.0 to 54.2 % by volume) and different grain size distribution. Experiments were performed first on the fraction finer than 0.075 mm and then on suspensions with fine sand (up to 0.425 mm in size and percentages varying from 10 to 50 %). A vane apparatus connected to a rotational rheometer was used. Three different samples from a debris flow deposit were used. The samples contained around 40–55 % Quartz and 35–51 % Illite with minor amounts of Clinichore, K-feldspar, Colostone and clay minerals. At low shear rates the experiments were well fitted to the Bingham as well as the Hershel-Bulkley models. For the fraction finer than 0.075 mm the yield stress increased from 80 to 1 100 Pa and Bingham viscosity increased from 1 to 20 Pa s when the solid s content increased from 37 to 48 %. The addition of up to 50 % sand (< 0.425 mm) influenced the rheologic properties surprisingly little. Fitting the data to the Hershel-Bulkley model gave values of the exponent n between 0.9 and 1.3. This slurry can be seen as a slightly non-Newtonian fluid.

Equation 4-1 shows the Bingham model and 4-2 the Herschel-Bulkley model

$$\tau = \tau_y + \eta_B \dot{\gamma} \quad (4\text{-}1)$$

$$\tau = \tau_y + K_{HB} \dot{\gamma}^n \quad (4\text{-}2)$$

τ is shear stress, τ_y is yield stress, η_B is Bingham viscosity, $\dot{\gamma}$ is shear rate, The constants n and K_{HB} are determined from experiments. When $n = 1$ the fluid is Newtonian and K_{HB} is viscosity.

Another candidate fine-grained material is Kaolinite, which is a non-swelling clay with mostly non-charged particles. Examples of three different Kaolinite properties of suspensions with particle sizes 1–60 µm with 30–40 % w/w solid content have Bingham yield stress of 10 to 80 Pa and Bingham viscosity of from 0.04 to 1 Pa s in circum-neutral waters (Nuntiya and Prasanphan 2006).

These values suggest that the yield stress will not more than marginally delay expansion but may slow down sedimentation in sloping fractures. The experimental techniques used by Sosio and Crosta (2009) could be used to measure CaMt and calcium bentonite rheology.

5 Water and ion transport in the rock matrix – rock matrix diffusion, RMD

5.1 Overview

The model used in this report assumes that the walls of the fractures are totally impregnable to flow and diffusion. This is not true for the crystalline rocks of interest here. The rock matrix has a connected porosity of around 0.1–0.5 %. The hydraulic conductivity is low, on the order of 10^{-14} m/s and the pore diffusion coefficient is on the order of 10^{-11} to 10^{-10} m^2/s (Neretnieks 1980). It plays an important role in retarding radionuclide transport in the fractured rock by allowing the nuclides that are transported by the seeping water to enter into and reside a while in the rock matrix. Rock matrix diffusion in Swedish crystalline rocks has been extensively studied experimentally in the laboratory as well as in field experiments down to and below repository depth (Löfgren and Neretnieks 2003), In this section we explore what impact rock matrix diffusion, RMD, may have on clay expansion and erosion in fractures that intersect the deposition hole. In previous modelling experiments of bentonite expansion into narrow fractures the two fracture walls have been impermeable. Bentonite expansion has been driven by the intrusion of ions and water from that in the seeping fracture itself. Exchange of ions between water and clay has been taking place only over the interface between clay and water in the fracture itself.

5.2 Ion diffusion through rock matrix to intersecting fracture

It was shown earlier, Chapter 4, that the seeping velocity of the water in the fracture practically always is sufficiently large to generate so low mass transfer resistance, (the inverse of Q_{eq}) that makes the smectite at the rim to be in ion-exchange equilibrium with the seeping water. For dilute waters it was found that X_{Ca} always would be well above 0.9 for large Δr. The smectite in the fracture closer to the DH can have X_{Ca} below 0.9. It is then swelling and will push the non-swelling clay near the IF outward.

We explore here how the RMD may affect the expansion. The rock matrix pore water has essentially the same composition as the seeping water in the fractures and will supply the clay that expands into the fractures with sufficient divalent calcium ions to attain X_{Ca} above 0.9 earlier than what the transport over only the IF does. This is demonstrated by a simple comparison of the rate of ion transport in the radial r-direction in the fracture and that in the z-direction perpendicular to the fracture.

Here we simplify the transport equation in the fracture to be linear instead of radial for two reasons. It is simpler and therefore easier for illustration purposes and it will be found that the extrusion distance likely will be so short that linear expansion is a very good approximation of radial expansion when the distance is less than the radius of the deposition hole. The ion transport rate in the radial direction, N_r in the fracture is

$$N_r = D_c \phi W \delta \frac{\Delta c_{Ca}}{\Delta r} \tag{5-1}$$

δ is aperture, W width of fracture, Δc_{Ca} is difference in c_{Ca} between that in the DH and that at the IF. Δr is expansion distance.

The transport rate of calcium through the rock matrix from some fracture not intersecting the fracture intersecting the deposition hole is approximated by

$$N_z = 2\, D_p \varepsilon_p W \Delta r \frac{\Delta c_{Ca}}{\Delta z} \quad (5\text{-}2)$$

The "2" stands for both sides of the fracture, D_p and ε_p are pore diffusion coefficient in rock matrix and ε_p is rock matrix porosity respectively. Δz is distance to nearest water bearing fracture not intersecting the DH.

The ratio of the two transport rates is

$$\frac{N_r}{N_z} = \frac{D_c \phi \delta \Delta z}{2 D_p \varepsilon_p \Delta r^2} \quad (5\text{-}3)$$

The rates are equal when

$$\Delta r = \sqrt{\frac{D_c \phi \delta \Delta z}{2 D_p \varepsilon}} \quad (5\text{-}4)$$

As an example with $D_c\phi = 10^{-11}$, $D_p\varepsilon_p = 10^{-14}$ m^2/s, $\delta = 10^{-4}$ m and $\Delta z = 10$ m the expansion distance at which the rates are equal $\Delta r = < 0.1$ m.

This suggests that rock matrix diffusion becomes important to influence the chemical composition and thus X_{Ca} for clay expansion beyond tens of cm and that expansion will be even less when only transport in the fracture water was accounted for. This is based on the hypothesis that smectite collapses when $X_{Ca} > 0.9$ and forms fine grains in the fracture that by mechanical friction resists further clay expansion.

6 Some further comments on wall friction

Smectite particles can be seen as very large molecules. A smectite paste can be conceived as a fluid consisting of two types of molecules, smectite particles and water molecules. When the paste is put in contact with water with a lower smectite concentration, e.g., pure water, the two fluids mix by molecular diffusion. The vacated volume by the smecite particles is replaced by an identical volume of water molecules. There is no wall friction because the mixture of the two liquids is stagnant. This is fully analogous to the mixing of two different miscible fluids. The mixing is caused by the thermally induced random movement of the molecules. Einstein's paper (Einstein 1905) based on arguments inspired by the observations of Brownian movement of microscopic particles in a fluid laid the theoretical foundation for Fick's laws.

In the smectite/water system there are other forces in addition to the thermal that act on the particles. The repulsive diffuse double layer repulsive force, DDL-force, makes the particles distance themselves from each other. The friction against the water restrains the movement and determines the rate. The rate of *dilution* of the smectite-water mixture can be described by an equation similar to the Einstein diffusion equation (Neretnieks et al. 2009, Liu 2010, 2011). This was verified experimentally by magnetic resonance imaging, MRI, experiments, over a wide range of smectite volume fractions (Dvinskikh and Furó 2009). The model and the experiments are also described in Neretnieks et al. (2009). That report, in an appendix, also summarizes our early arguments for why there is no wall friction involved in the dilution of a pure smectite-water mixture as it is *diluted* in even very thin fractures.

The smectite particles actually are not in direct physical contact with the electrically neutral wall. If not collapsed in stacks at high X_{Ca} they keep a distance that is half the distance between the smectite particles at a given swelling pressure, when aligned parallel to the wall but also when perpendicular to it. Even the stacks repel each other at more than 5 % volume fraction smectite.

Bentonites contain small grains of other minerals that are non-charged. These minerals can touch the walls on the fractures and can exert mechanical wall friction when they slide along it as they are pressed against the wall by the swelling smectite. The grains can roll along the wall also and then have to be "lifted." out of the microscopic depression of the wall. It is even conceivable that the fine "sand" particles will tend to concentrate near the wall because this will release more volume for the smectite particles. If this would increase or decrease any wall friction is open to debate.

There is additional experimental evidence that smectite poor in sand will not be influenced by the aperture size, Alonso et al. (2019) found that in 0.2, 0.4 and 1 mm aperture fractures the clay expanded the same distance. On the other hand, experiments with a Japanese bentonite with more than 50 % fine sand expanded very differently in 1 and in 1.5 mm aperture fractures (Kanno et al. 2001).

Swelling experiments in large diameter tubes with a natural bentonite show that full redistribution of swelling pressure between different volume fraction clay in two ends of the tube is not reached over many years. Non-equal steady state pressure profile is reached much earlier (Dueck et al. 2018).

Börgesson et al. (2018) using the concept of mechanical friction conclude: "Depending on the approach taken and the swelling pressure chosen the evaluated friction angles show large variations, 0.5 to 30°. However, by using these large variations in the sensitivity analyses we were able to show that the penetration into a 100 μm wide fracture is anyway limited to < 80 mm at the lowest friction angle. Comparison between theory and experimental swelling of Wy-Na into a 120 μm fracture gives best agreement for the highest friction angle, 30° which gave a penetration depth in the vicinity of 1 mm. Thus, we can conclude that above the CCC bentonite swelling into fractures is limited to distances very much smaller than the deposition hole diameter. Other tests above and below CCC have confirmed this conclusion."

We conclude that the mechanisms underlying wall friction are not well understood. Because wall friction could have important effects on the expansion and erosion of bentonite in fractures intersecting deposition holes, drifts and tunnels it should be better studied further on theoretical grounds as well as with experiments.

7 Discussion and conclusions

7.1 Discussion

The model described in Chapter 4 is based on well-known processes but also on some simplifying assumptions that must be experimentally validated. It is modelled how the clay that expands is affected by the presence of ten(s) of percent of other minerals and how that may influence the (expansion), actually dilution, of the smectite as it diffuses into the water in the fracture. It has been suggested that the clay dilution could be impeded by mechanical friction. This is projected to limit the expansion to at most 8 cm in 0.1 mm fracture apertures (Börgesson et al. 2018). Some experiments that illuminate the underlying physics would be of value.

There is a very narrow region of ionic strengths and ion compositions at which bentonite clay can release smectite particles into seeping groundwater in fractures to form colloidal sol. One extreme is water formed from glacial melt-waters. Passing the rock, they collect one to a few mM dissolved mineral salts. In such waters the smectite will collapse into stacks that are too heavy to solubilize. The slurry of stacks could conceivable impede the expansion of the clay into the fracture. Dilute waters allow the clay at the clay water interface, IF, to a attain $X_{Ca} > 0.9$ after some metres expansion into the fracture by capturing and incorporating calcium ions from the water into ion exchange positions. The hypothesis that the collapsed smectite stacks at $X_{Ca} > 0.9$ might form a slurry that impedes expansion of the swelling clay behind must be experimentally verified. Better data on the rheologic properties of such slurries is needed.

At ionic strengths larger than some tens of mM salts with typical ion compositions the smectite cannot form a sol because this is above the critical coagulation concentration, CCC. In below CCC waters the "spontaneous" floc formation and later de-flocculation is observed in experiments but the reasons for this are not well understood. We have found no reliable quantitative model to use in simulating these phenomena for smectite sols in fractures.

In even more saline waters sol formation cannot occur and swelling will cease at lower volume fractions smectite.

The common assumption in modelling and in laboratory experiments that fracture walls are impermeable is conservative in the sense that the $X_{Ca} > 0.9$ is more rapidly attained by calcium diffusion also through the porous rock matrix to the clay in the fracture.

7.2 Conclusions

The ion transport in bentonites and smectite including ion exchange rates and mechanisms are well understood and can be quantified. Acknowledging that there are large variations and uncertainties in data, calcium and sodium ions are the most important species. Their concentration in clay and water suffice to determine the swelling pressure, coagulation, sol formation and stack collapse of the smectite particles.

Floc formation and later sol re-formation are understood qualitatively but it is difficult to model their behaviour quantitatively in narrow aperture fractures.

Observations in several experiments suggest that the presence of the secondary mineral particles in bentonite influence the expansion of clay in slits and tubes and can even help clogging variable aperture fractures. The underlying physics and clogging mechanism are insufficiently studied and understood.

One important finding in the present study is that at most few metres of clay expansion into a fracture ensure that the clay cannot solubilise in dilute groundwaters.

8 Possible experiments for model testing/validation

Experiments

As noted earlier there is scant information on the rheology of slurries with $X_{Ca} > 0.9$. This is essential to assess to what degree a slot filled with smectite can hinder/retard further expansion of clay into the fracture.

Proposed experiment 1

Measure rheology of smectite with $X_{Ca} > 0.9$, and fit to Bingham, Hershel-Bulkeley models. See Section 4.3.

Proposed experiment 2

Make experiments with smectite $X_{Ca} > 0.9$ slurry flow in narrow (0.1 and 0.2 mm) fractures and/or capillaries to verify yield stress and flow viscosity in actual slit flow.

Exploratory idea of a demonstration experiment

In Chapter 5 it was shown that the transport of calcium from and through the pores of the rock matrix could contribute to the generation of $X_{Ca} > 0.9$ conditions also if the pore water is dilute. We explored the following idea. To test that calcium transport from dilute waters by diffusion through the rock matrix can make the smectite in a slot attain $X_{Ca} > 0.9$ much closer to the deposition hole the following experiments could be made.

Experiment 3

A thin slit between a granite slab and glass filled with slurry of $X_{Ca} << 0.9$ smectite is exposed to Grimsel water on the granite side. Visual and microscopic photos follow if and how the slurry develops a grainy structure. A post mortem measures the X_{Ca} of the slurry. If successful a direct simulation of expansion of clay into a fracture can be made as follows.

Experiment 4

One side of the slit is in contact with a “large” volume of compacted bentonite simulating the deposition hole. The granite is in contact with “Grimsel“ water. The side of the slit opposite to the compacted smectite is “flushed” with Grimsel water. Visually and by microscope photos one could observe how smectite expands into the slit and forms a grainy structure. This would be an indication that $X_{Ca} > 0.9$. See Section 5.2. Another parallel experiment with a slit between two glass sheets is also made for comparison.

Scoping visual & microscope photos of thin smectite slurry layers with X_{Ca} below and above 0.9 showed no clear differences in structure. This is actually not surprising because smectite stacks with $X_{Ca} > 0.9$ even with hundreds of sheets are smaller than the wavelength of visible light. The smectite stacks must form larger agglomerates and develop a grainy structure to be visible.

Summary of the thoughts on experiments.

Experiment 1 is seemingly simple but not straight forward as was found by Clay Technology as the $X_{Ca} > 0.9$ slurry sediments (Birgersson et al. 2009). Experiment 2 needs development of the experimental setup. The setup for experiment 3 also needs to be designed so that a reasonable experimental time can be assured to give results. Experiment 4 is very complex and needs careful design. With luck it could be a nice demonstration to give support to the modelling, which must run in parallel.

9 Notation

A_{slit}	Cross section of aperture	m^2
c	Concentration in water	mol/m^3 (= mM)
$c_{An,tot}$	Anion concentration as charge equivalents	eqv/m^3 eqv/m^3
CEC	Ion exchange capacity	eqv/kg
D_{clay}	Diffusion coefficient of smectite	m^2/s
D_{FW}	Diffusion coefficient in “Free Water”	m^2/s
D_p	Diffusion coefficient in pore water	m^2/s
D_q	Diffusion coefficient in X-Phase	m^2/s
D_w	Diffusion coefficient in unconfined water	m^2/s
D_X	Defined in Equation 3-7	eqv/s
J_i	Flux of component “i”	$mol/m^2/s$
K_{CaNa}	Equilibrium coefficient	mM
N_i	Flowrate of component “i”	mol/s
N_r	Flowrate in r-direction	mol/s
N_z	Flowrate in z-direction	mol/s
q	Concentration in X-phase	mol/m^3 clay
r	Radial coordinate	r
u_w	Water velocity	m/s
W	Width of section of fracture	m
x	x-coordinate	m
X_i	Fraction of charge bound by cation “i” in X-phase	-
z	z-coordinate, perpendicular to fracture	m
$\dot{\gamma}$	Shear rate	s^{-1}
δ	Fracture aperture	m
ε_{FW}	Fraction of all water defined as “Free Water”	-
η_B	Bingham viscosity	Pa s
τ	Shear stress	Pa
τ_y	Yield stress	Pa
ϕ	Volume fraction	

Subscripts

An	Anion
Ca	Calcium
Na	Sodium
w	Water
GW	Groundwater
IF	Interface
DH	Deposition hole

References

SKB's (Svensk Kärnbränslehantering AB) publications can be found at www.skb.com/publications.

Abend S, Lagaly G, 2000. Sol-gel transitions of sodium montmorillonite dispersions. Applied Clay Science 16, 201–227.

Adachi Y, Di C, Xiao F, Kobayashi M, 2019. Size, orientation, and strength of Na-montmorillonite flocs flowing in a laminar shear flow. Colloid and Polymer Science 297, 979–987.

Alonso U, Missana T, Gutiérrez M G, Morejón J, Mingarro M, Fernández A M, 2019. CIEMAT studies within POSKBAR project. Bentonite expansion, sedimentation and erosion in artificial fractures. SKB TR-19-08, Svensk Kärnbränslehantering AB.

Alt-Epping P, Gimmi T, Wersin P, Jenni A, 2018. Incorporating electrical double layers into reactive-transport simulations of processes in clays by using the Nernst–Planck equation: A benchmark revisited. Applied Geochemistry 89, 1–10.

Bergaya F, Theng B K G, Lagaly G (eds), 2006. Handbook of clay science. Amsterdam: Elsevier.

Bird R B, Stewart W E, Lightfoot E N, 2002. Transport phenomena. 2nd ed. New York: Wiley.

Birgersson M, Karnland O, 2009. Ion equilibrium between montmorillonite interlayer space and an external solution—Consequences for diffusional transport. Geochimica et Cosmochimica Acta 73, 1908–1923.

Birgersson M, Börgesson L, Hedström M, Karnland O, Nilsson U, 2009. Bentonite erosion. Final report. SKB TR-09-34, Svensk Kärnbränslehantering AB.

Birgersson M, Hedström M, Karnland O, 2011. Sol formation ability of Ca/Na-montmorillonite at low ionic strength. Physics and Chemistry of the Earth, Parts A/B/C 36, 1572–1579.

Bourg I C, Sposito G, 2011. Ion exchange phenomena. In Huang P M, Li Y, Sumner M E (eds). Handbook of soil sciences. Properties and processes. 2nd ed. Boca Raton, FL: CRC Press.

Bourg I C, Bourg A C M, Sposito G, 2003. Modeling diffusion and adsorption in compacted bentonite: a critical review. Journal of Contaminant Hydrology 61, 293–302.

Bourg I C, Sposito G, Bourg A C M, 2018. Modeling the diffusion of Na+ in compacted water-saturated Na-bentonite as a function of pore water ionic strength. Applied Geochemistry 23, 3635–3641.

Brown G H, 2002. Glacier meltwater hydrogeochemistry. Applied Geochemistry 17, 855–883.

Börgesson L, Hedström M, Birgersson M, Karnland O, 2018. Bentonite swelling into fractures at conditions above the critical coagulation concentration. SKB TR-17-11, Svensk Kärnbränslehantering AB.

Cadene A, Durand-Vidal S, Turq P, Brendle J, 2005. Study of individual Na-montmorillonite particles size, morphology and apparent charge. Journal of Colloid and Interface Science 285, 719–730.

Dueck A, Goudarzi R, Börgesson L, 2018. Buffer homogenisation – status report 4. SKB TR-17-04, Svensk Kärnbränslehantering AB.

Dvinskikh S V, Furó I, 2009. Magnetic resonance imaging and nuclear magnetic resonance investigations of bentonite systems. SKB TR-09-27, Svensk Kärnbränslehantering AB.

Einstein A, 1905. Über die von der molekularkinetischen Theorie der Wärme geforderte Bewegung von in ruhenden Flüssigkeiten suspendierten Teilchen. Annalen der Physik 322, 549–560. (In German.)

Evans D F, Wennerström H, 1999. The colloidal domain: where physics, chemistry, biology, and technology meet. 2nd ed. New York: Wiley.

Gimmi T, Alt-Epping P, 2018. Simulating Donnan equilibria based on the Nernst-Planck equation. Geochimica et Cosmochimica Acta 232, 1–13.

Glaus M A, Aertsens M, Appelo C A J, Kupcik T, Maes N, Van Laer L, Van Loon L R, 2015. Cation diffusion in the electrical double layer enhances the mass transfer rates for Sr^{2+}, Co^{2+} and Zn^{2+} in compacted illite. Geochimica et Cosmochimica Acta 165, 376–388.

Glaus M A, Frick S, Van Loon L R, 2020. A coherent approach for cation surface diffusion in clay minerals and cation sorption models: Diffusion of Cs^{+} and Eu^{3+} in compacted illite as case examples. Geochimica et Cosmochimica Acta 274, 79–96.

Hedström M, Ekvy-Hansen E, Ulf Nilsson U, 2016. Montmorillonite phase behaviour. Relevance for buffer erosion in dilute groundwater. SKB TR-15-07, Svensk Kärnbränslehantering AB.

Idiart A, Pękala M, 2016. Models for diffusion in compacted bentonite. SKB TR-15-06, Svensk Kärnbränslehantering AB.

Idiart A, Coene E, Bagaria, F, Román-Ross G, Birgersson M, 2019. Reactive transport modelling considering transport in interlayer water. New model, sensitivity analyses and results from the Integrated Sulfide Project inter-model comparison exercise. SKB TR-18-07, Svensk Kärnbränslehantering AB.

Israelachvili J N, 2011. Intermolecular and surface forces. 3rd ed. Burlington: Academic Press.

Jönsson B, Åkesson T, Jönsson B, Meehdi M S, Janiak J, Wallenberg R, 2009. Structure and forces in bentonite MX-80. Theoretical Chemistry, Chemical Center, Lund, Sweden.

Kanno T, Iwata Y, Sugino H, 2001. Modelling of bentonite swelling as solid particle diffusion. In Adachi K, Fukue M (eds). Clay science for engineering. Boca Raton, FL: CRC Press, 561–570.

Karnland O, Muurinen A, Karlsson F, 2003. Bentonite swelling pressure in NaCl solutions, Experimentally determined data and model calculations. In Advances in understanding engineered clay barriers. Proceedings of the international symposium on large scale field tests in granite, Barcelona, Spain, 12–14 November 2003, 241–256.

Karnland O, Olsson S, Nilsson U, 2006. Mineralogy and sealing properties of various bentonites and smectite-rich clay materials. SKB TR-06-30, Svensk Kärnbränslehantering AB.

Kjellander R, Marcelja S, 1988. Attractive double-layer interactions between calcium clay particles. Journal of Colloid and Interface Science 12, 194–211.

Kozaki T, Fujishima A, Saito N, Sato S, Ohashi H, 2005. Effects of dry density and exchangeable cations on the diffusion process of sodium ions in compacted montmorillonite. Engineering Geology 81, 246–254.

Laxton P B, Berg J C, 2006. Relating clay yield stress to colloidal parameters. Journal of Colloid and Interface Science 296, 749–755.

Liu L, 2010. Permeability and expansibility of sodium bentonite in dilute solutions. Colloids and Surfaces A: Physicochemical and Engineering Aspects 358, 68–78.

Liu L, 2011. A model for the viscosity of dilute smectite gels. Physics and Chemistry of the Earth, Parts A/B/C 36, 1792–1798.

Liu L, 2013. Prediction of swelling pressures of different types of bentonite in dilute solution. Colloids and Surfaces A: Physicochemical and Engineering Aspects 434, 303–318.

Liu L, Moreno L, Neretnieks I, 2009a. A dynamic force balance model for colloidal expansion and its DLVO-based application. Langmuir 25, 679–687.

Liu L, Moreno L, Neretnieks I, 2009b. A novel approach to determine the critical coagulation concentration of a colloidal dispersion with plate-like particles. Langmuir 25, 688–697.

Löfgren M, Neretnieks I, 2003. Formation factor logging by electrical methods: Comparison of formation factor logs obtained in situ and in the laboratory. Journal of Contaminant Hydrology 61, 107–115.

Missana T, Alonso U, Turrero M J, 2003. Generation and stability of bentonite colloids at the bentonite/granite interface of a deep geological radioactive waste repository. Journal of Contaminant Hydrology 61, 17–31.

Missana T, Alonso U, Albarran N, García-Gutiérrez M, Cormenzana J-L, 2011. Analysis of colloids erosion from the bentonite barrier of a high level radioactive waste repository and implications in safety assessment. Physics and Chemistry of the Earth 36, 1607–161.

Molera M, Eriksen T, 2002. Diffusion of $^{22}Na^{+}$, $^{85}Sr^{2+}$, $^{134}Cs^{+}$ and $^{57}Co^{2+}$ in bentonite clay compacted to different densities: experiments and modeling. Radiochimica Acta 90, 753–760.

Moreno L, Neretnieks I, Liu L, 2010. Modelling of erosion of bentonite gel by gel/sol flow. SKB TR-10-64, Svensk Kärnbränslehantering AB.

Moreno L, Liu L, Neretnieks I, 2011. Erosion of sodium bentonite by flow and colloid diffusion. Physics and Chemistry of the Earth, Parts A/B/C 36, 1600–1606.

Neretnieks, I, 1980. Diffusion in the rock matrix: An important factor in radionuclide retardation? Journal of Geophysical Research 85, 4379–4397.

Neretnieks I, 2019. Density driven mass transfer in repositories for nuclear waste. SKB R-18-05, Svensk Kärnbränslehantering AB.

Neretnieks I, Moreno L, 2018. Revisiting bentonite erosion understanding and modelling based on the BELBaR project findings. SKB TR-17-12, Svensk Kärnbränslehantering AB.

Neretnieks I, Winberg-Wang H, 2019. Density-driven mass transfer in repositories for nuclear waste, nuclear technology. Nuclear Technology 205, 819–829.

Neretnieks I, Liu L, Moreno L, 2009. Mechanisms and models for bentonite erosion. SKB TR-09-35, Svensk Kärnbränslehantering AB.

Neretnieks I, Liu L, Moreno L, 2010. Mass transfer between waste canister and water seeping in rock fractures. Revisiting the Q-equivalent model. SKB TR-10-42, Svensk Kärnbränslehantering AB.

Neretnieks I, Moreno L, Liu L, 2017. Clay erosion – impact of flocculation and gravitation, SKB TR-16-11, Svensk Kärnbränslehantering AB.

Nuntiya A, Prasanphan S, 2006. The rheological behavior of kaolin suspensions. Chiang Mai Journal of Science 33, 271–281.

Paineau E, Michot L J, Bihannic I, Baravian C, 2011. Aqueous suspensions of natural swelling clay minerals. 2. Rheological characterization. Langmuir 27, 7806–7819.

Parkhurst D L, Appelo C A J, 1999. User's guide to PHREEQC (version 2): a computer program for speciation, batch-reaction, one-dimensional transport, and inverse geochemical calculations. Water-Resources Investigations Report 99-4259, U.S. Geological Survey, Denver, Colorado.

Posiva, 2012. Safety case for the disposal of spent nuclearfuel at Olkiluoto – Design basis 2012. Posiva 2012-3, Posiva Oy, Finland.

Pujala R K, 2014. Dispersion stability, microstructure and phase transition of anisotropic nanodiscs. Cham: Springer International Publishing.

Pusch R, Yong R N, 2006. Microstructure of smectite clays and engineering performance. London: Taylor & Francis.

Reid C, Lunn R, El Mountassir G, Tarantino A, 2015. A mechanism for bentonite buffer erosion in a fracture with a naturally varying aperture. Mineralogical Magazine 79, 1485–1494.

Richards T, Neretnieks I, 2010. Filtering of clay colloids in bentonite detritus material. Chemical Engineering & Technology 33, 1303–1310.

Ruzicka B, Zaccarelli E, Zulian L, Angelini R, Sztucki M, Moussaïd A, Narayanan T, Sciortino F, 2011. Observation of empty liquids and equilibrium gels in a colloidal clay. Nature Materials 10, 56–60.

Sakairi N, Kobayashi M, Adachi Y, 2005. Effects of salt concentration on the yield stress of sodium montmorillonite suspension. Journal of Colloid and Interface Science 283, 245–250.

Salas J, Gimeno M J, Auqué L, Molinero J J, Gómez J, Juárez I, 2010. SR-Site – hydrogeochemical evolution of the Forsmark site, SKB TR-10-58, Svensk Kärnbränslehantering AB.

Sato H, Ashida T, Kohara Y, Yui M, Sasaki N, 1992. Effect of density on diffusion of some radionuclides in compacted sodium bentonite. Journal of Nuclear Science and Technology 29, 873–882.

Schatz T, Akhanoba N, 2017. Buffer erosion in sloped fracture environments. Posiva 2016-13, Posiva Oy, Finland.

Schatz T, Kanerva N, Martikainen J, Sane P, Olin M, Seppälä A, Koskinen K, 2013. Buffer erosion in dilute groundwater. Posiva 2012-44, Posiva Oy, Finland.

Schatz T, Eriksson R, Ekvy Hansen E, Hedström M, Missana T, Alonso U, Mayordomo N, Fernández A M, Bouby M, Heck S, Geyer F, Schäfer T, 2015. WP2 partners final report on bentonite erosion. Deliverable D2.11, European Commission.

Shalkevich A, Stradner A, Bhat S K, Muller F, Schurtenberger P, 2007. Cluster, glass, and gel formation and viscoelastic phase separation in aqueous clay suspensions. Langmuir 23, 3570–3580.

SKB, 2010. Geosphere process report for the safety assessment SR-Site. SKB TR-10-48, Svensk Kärnbränslehantering AB.

SKB, 2011. Long-term safety for the final repository for spent nuclear fuel at Forsmark Main report of the SR-Site project. SKB TR-11-01, Svensk Kärnbränslehantering AB.

Sosio R, Crosta G B, 2009. Rheology of concentrated granular suspensions and possible implications for debris flow modeling. Water Resouces Research 45, W03412. doi:10.1029/2008WR006920

Tinnacher R M, Holmboe M, Tournassat C, Bourg I C, Davis J A, 2016. Ion adsorption and diffusion in smectite: Molecular, pore, and continuum scale views. Geochimica et Cosmochimica Acta 177, 130–149.

Tournassat C, Appelo C A J, 2011. Modelling approaches for anion-exclusion in compacted Na-bentonite. Geochimica et Cosmochimica Acta 75, 3698–3710.

van Olphen H, 1977. An introduction to clay colloid chemistry: for clay technologists, geologists, and soil scientists. 2nd ed. New York: Wiley.

Van Loon L R, Glaus M A, Müller W, 2007. Anion exclusion effects in compacted bentonites: Towards a better understanding of anion diffusion. Applied Geochemistry 22, 2536–2552.

Wang Z, Liu L, Neretnieks I, 2011. A novel method to describe the interaction pressure between charged plates with application of the weighted correlation approach. The Journal of Chemical Physics 135, 244107. doi:10.1063/1.3672001

Yang G, Neretnieks I, Holmboe M, 2017. Atomistic simulations of cation hydration in sodium and calcium montmorillonite nanopores. The Journal of Chemical Physics 147, 084705. doi:10.1063/1.4992001

Appendix A

Erosion of bentonite buffer in radwaste repositories – potential for gel and detritus to clog fractures

A1 Introduction and background

A1.1 The context

Bentonite clay will be used as buffer and backfill material to protect the copper canisters that contain the highly radioactive spent nuclear fuel from the Swedish and Finnish nuclear reactors. The repositories are located at about 500 m depth in crystalline rocks. Highly compacted bentonite surrounds and protects the canisters. The bentonite swells by intruding water and only allows negligible water flow to contact the canister. Corrosive agents may diffuse through the swollen bentonite but in negligible quantities. Should, however, the canister be damaged the bentonite slows down the escape of radionuclides to the seeping groundwater in the fractured rock. Leakage of nuclides to the biosphere must be hindered for more than hundreds of thousands of year. There are concerns that very dilute waters will solubilise the mmt in the bentonite and that it could be lost to the seeping water in sufficient amounts to impair its protective function.

Figure A1-1 Illustrates the concepts underlying the erosion of clay from a deposition hole in the KBS-3 repository as envisaged in Neretnieks et al. (2009). The compacted clay expands pushing the small accessory mineral particles, detritus, which are left behind when the mmt forms sol and is carried away by the seeping water. Neretnieks et al. (2009) developed a model, supported by experiments that showed how the clay expands in dilute waters and forms mmt sol that is carried away.

In modelling the bentonite loss in the performance assessments of the repositories by the Swedish and Finnish organisations responsible for building the repositories, SKB and Posiva respectively, any possible beneficial clogging of the fractures by detritus was not accounted for (SKB 2011, Posiva 2012).

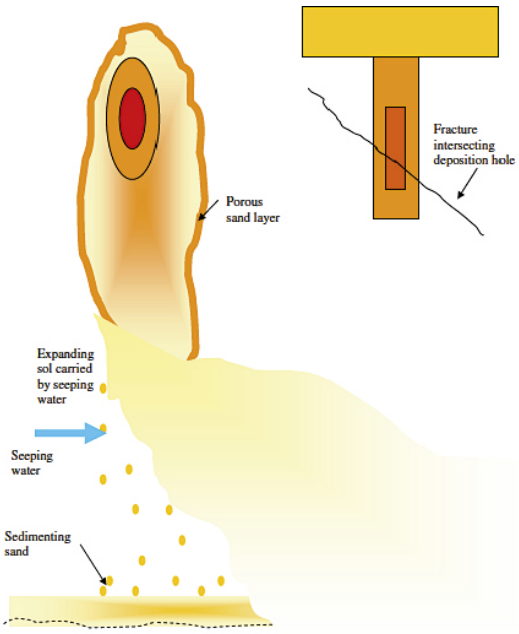

Figure A-1. *Illustration of how sand consisting of detritus particles could develop a filter in a fracture around a deposition hole or drift. The sand could be breached and sediment to the bottom of the fracture (Neretnieks et al. 2009).*

The expansion and erosion of mmt was described by a model in which the mmt platelets/sheets in the bentonite expand by the repulsive osmotic forces forcing the mmt platelets apart at a rate balanced by the friction of the platelets against the intruding water. In low ionic strength water the platelets eventually disperse by random Brownian diffusion. The suspension becomes a sol. This is in contrast to what happens at higher ionic strength. Then van der Waals forces stop the sol formation and gel is formed. The model also predicts the ionic strength, the critical coagulation concentration CCC at which gel forms. This model is supported by experiments and observations. However, as demonstrated later that over time scales of interest for nuclear waste repositories the mmt sol is unstable.

A1.2 Aims

One aim is to study the impact of the recently growing evidence that mmt sol, which was expected to be stable in low ionic strength water is not. It "rapidly" forms flocs that phase separate into gel and clear water. The gel is highly viscous and will aid to clog fractures. Another aim is to explore whether the detritus, which makes up for ten(s) of percent of bentonites can be expected to form filters that clog the narrow, < 0.1 mm, variable aperture fractures in the rock.

A1.3 Some recent observations of unstable sols

Experiments by Schatz et al. (2013) showed that the colloidal particles in sol agglomerate and form flocs that flow with the water. This was entirely unexpected in the dilute waters where the ionic strength is well below the critical coagulation concentration, CCC, under which conditions sol is expected to be stable. The erosion model was modified to include floc formation and the flow of water containing flocs. Floc formation will speed up the erosion rate if the flocs move away and allow new colloid particles to be release at the clay/water interface (Neretnieks et al. 2017). Schatz and Akhanoba (2017) showed that the flocs grow and form coherent gel even in very dilute waters. This gel moves very slowly in the narrow fractures.

Schatz et al. (2013) and Schatz and Akhanoba (2017) found in experiments in which pellets expanded in horizontal narrow slots into seeping deionised water, DI, and other dilute waters that the mmt initially formed sol as expected but that the sol gradually formed flocs that flowed with the water. After turning the slots vertical or 45 degrees the flocs sediment in the gravity field and collect in heaps at the bottom of the slot. The expansion rate of mmt into the slot and the rate of loss could not be predicted by the dynamic model unless rapid agglomeration of mmt was assumed to occur and if the flocs flow unimpeded with the seeping water, Neretnieks et al. (2017). The Schatz and Akhanoba (2017) experiments also suggest that the heaps of sedimented flocs at the bottom of the slot do not collapse, suggesting that the sediments develop a yield strength with time. The experiments also show that in narrow vertical slots (0.1 mm) the sedimenting flocs collect and grow during their passage and come in contact with the walls, slowing down the sedimentation. The moving sediment forms a coherent agglomerate fluid, AF, which has a higher viscosity than water and moves slower. For predictive modelling of the movement of the AF, its rheologic properties and how these evolve over time are needed.

A1.4 Short overview of properties of suspensions, flocs and gels

The rheology of the AF is a key property that determines its rate of movement. There is a need to gain understanding of the conditions and mechanisms for floc and sediment formation in below CCC waters and how this influences clay loss from deposition holes. Central questions are *yield strength* and *apparent viscosity* of gels and sediments in low ionic strength waters.

Abend and Lagaly (2000) measured the yield strength and apparent viscosity of four freshly prepared detritus free sodium mmt suspensions at NaCl concentrations down to 0.01 mM. The yield strengths of 2 % by weight, W%, mmt varied between 0.1 and about 1 Pa for NaCl concentrations below 10 mM. Sakairi et al. (2005) measured yield strength with the vane method on mmt suspensions with volume fractions between 0.6 and 2 V% and found yield strengths increasing from 1 to 100 Pa in this range for NaCl concentrations below 1 mM. (1 $W\% \cong 2.7 \times V\%$). For 5 and 10 mM waters there was a sharp increase of yield strength between 1–2 V% mmt. Birgersson et al. (2009) reported yield strengths for sodium exchanged mmt as well as for as-received MX-80 bentonite from Wyoming in dilute waters. Yield strength increased strongly with increasing W% of clay and was about 1 Pa at 3 W% and 10 Pa at 5 W% in distilled water. The yield strength increased with resting, more for the denser clays. All these

data were obtained by measuring yield strength either immediately or after a short time after suspending mmt in water. In none of these papers is there mention of gel forming in low ionic strength, low W% waters. (Paineau et al. 2011) measured yield strength of different clay suspensions including a Wyoming bentonite. All experiments were made at 1 mM NaCl and lower ionic strengths, to ensure below CCC conditions. Volume fractions varied between 0.58 and 1.53 V% for the Wyoming clay. The yield strength increased from between 0 and 3 to about 50 Pa in this volume fraction span. At volume fraction 0.58 the yield strength was zero, an indication that Newtonian conditions were approached. The samples were freshly prepared and not allowed to age and no phase separation was reported. Suspensions of mmt below about 1 V% have no yield strength and behave as Newtonian fluids (Liu 2011).

A2 Phase separation of mmt sols

A2.1 Flocculation and gel formation

It is long known that in very low ionic strength waters, particle flocculation does occur but at an extremely slow rate. At higher but still low, 12–16 mM NaCl concentrations, flocs develop within minutes (van Olphen 1977). This is deemed to be because under some conditions the edges of mmt particles are positively charged and that one can expect complex 3D house of cards like structures, HoC, to develop and form gels (van Olphen 1977), Abend and Lagaly 2000, Laxton and Berg 2006). Other structures including chains of Edge to Edge, EE, bound particles have also been proposed. It is also possible that Edge to Face, EF bonds are also formed by van der Waals forces. Different and opposing views exist of how the complex 3D networks of sheet-like colloidal particles can form coherent structures of very different and sometimes extremely low volume fractions. Paineau et al. (2011) give an overview of the different views and interpretations. Their brief review of the literature clearly shows that the gelation mechanisms of swelling clays are still far from well understood and that different investigations using different techniques, preparation and observation modes and times can lead to contradicting conclusions.

An example of an extremely sparse gel is described by Hedström et al. (2016). The mmt gel that formed in semi-dilute water, 15 mM NaCl, at pH 11 has a volume fraction of 0.07 %. The gel is stable and supports its own weight for many years. Examples in which, at very low ionic strength, gels with much larger volume fractions form by sedimentation from suspensions are presented by Pujala (2014). He reported phase separation of mmt sol in deionised, DI, water at around pH = 8 in test tubes. At 3 W% no separation was observed. At 2.5 W%, sediment formed with a volume in the tube that is about 20 % of the original suspension volume. From his pictures it is seen that in the 3.5 year old sediment the supernatant is not quite clear and its mmt content cannot be accurately determined. Nevertheless the results show that the sediment contains much more than the starting 2.5 W%, probably up to 10 W% mmt. Approximately the same mmt concentration in the sediment resulted also starting with suspensions of 0.3, 0.5, 1.0, 1.5, and 2.0 W%. Neither the yield strength of the sediments nor other rheologic properties were measured.

Although it is expected that the yield strength of gels formed by phase separation will be different from newly prepared mmt suspensions with the same concentrations, rheology information of the latter is useful because sedimented gel that has been re-mobilised is expected to have similar flow properties as a freshly formed suspension.

In order to explore the properties of the phase separated sediment, a series of simple scoping experiments were performed with Wyoming MX-80 in de-ionised water, from which most of the non-soluble detritus material was removed by sedimentation. A commercial, detritus free, mmt, Nanocor, was also used.

A2.2 Experimental

For the experiments, 10.5 g Wyoming bentonite, MX-80, in 500 ml de-ionised water was vigorously shaken for 25 minutes and set to sediment for 3 hours and 15 minutes. The opaque supernatant was decanted leaving 30 ml sediment, which was evaporated and dried. It contained 3.86 g solid matter. The supernatant contains 6.64 g mmt with very small amounts of detritus particles. This supernatant has 1.4 W% mmt, and a volume fraction of 0.52 %. Microscope pictures of evaporated drops of the supernatant showed very few, very small particles in contrast to what was seen of the samples from the 30 ml first sediment.

In this stock suspension the mmt-free water had a pH of 8.6. It contained 408 mg/l salts. The conductivity was 563 μS/cm. If the salt would be only NaCl this would give a concentration around 7.0 mM. This is in itself interesting because it is well below the CCC of about 15–20 mM at which gel formation should not occur according to the conventional CCC models and as confirmed by extensive test reported in Hedström et al. (2016).

For the tests in small test tubes the stock suspension was vigorously re-suspended. The stock suspension is denoted **#2.** In one experiment 5 ml re-suspended stock suspension was mixed with 5 ml DI in a test tube. This tube is numbered **#3**. The tube was set vertical to sediment. Another tube, **#5**, with 1 ml of the stock suspension and 9 ml DI was prepared. In the tubes sediments with 2–4 V% had settled after less than one weak. The uncertainty in volume fraction is because it is estimated by measuring the height in the curved part of the bottom of the test tube and is very sensitive to errors in these measurements. The sediments in **#3** and **#5** are shown in Figure A-2. The mmt amount in **#5** is 5 times less than in **#3**. In both cases when the tubes were turned nearly horizontal the sediment did no move for many hours but some time overnight it has slid down. This is shown in the rightmost picture in Figure A-2.

Table A-1. Summary of the conditions in the tests.

	#2 Stock solution	#3	#4	#5
V% mmt at start	0.52	0.26	0.52	0.052
mM Na^+	7.0	3.5	7.0	0.7
Vol % sediment		About 3	About 3	About 3

These simple experiments confirm phase separation and that formation of gel-like structure occurs in ion concentrations well below what is conventionally thought to give stable sol. They also show that the sediment of the flocs has become extremely viscous, even if not a fully stable gel or Bingham body, after a few days consolidation.

Another test tube **#4** was prepared with the stock solution. It differs from the two other in that no dilution was done and that the test tube was gently rolled back and forth during one hour to promote flocculation No flocculation was observed during the rest of the day but a loose sediment had formed overnight in the tube set at an angle of 45°. Tilting from 45° to vertical did not change the slope of the sediment during the rest of the day. The slope changed later but it was not noted when. Six days later the tube was tilted to nearly horizontal position.

Figure A-3 shows pictures of the bottom of the tube **#4** at different times.

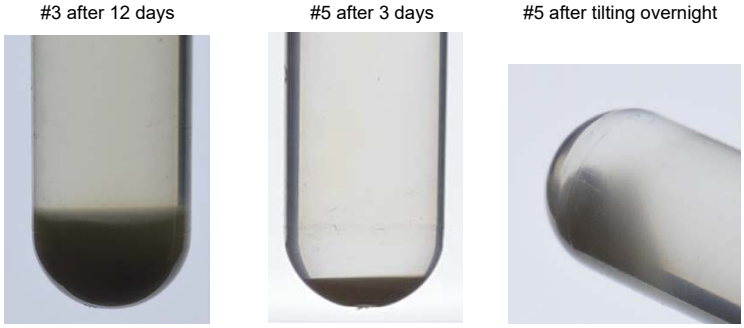

Figure A-2. *Sediments in water with about 3 mM (left) and 0.7 mM ion concentrations, the right two pictures.*

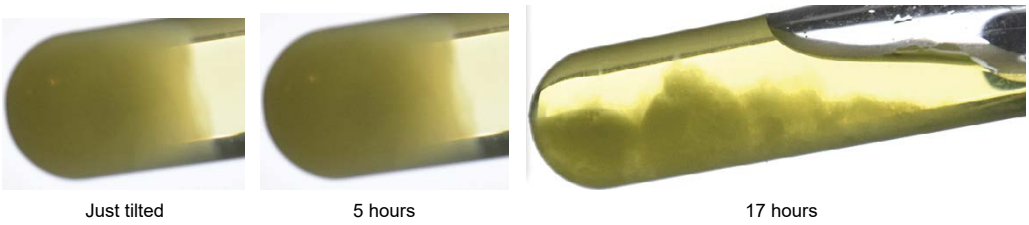

Figure A-3. *Behaviour of sediment in tube* ***#4*** *after tilting. Ion concentration about 7 mM.*

The sediment was rigid at first but after some time lost coherence and flowed out. When again tilted vertically the sediment "immediately" settled to give horizontal upper surface. However, the sediment had become a little less dense. Titling it vertical again, after about a week re-formed a horizontal gel/water interface with the earlier height. Two months later it had gained such strength that tilting it horizontal the interface remained vertical. This suggests that it takes more than a week to form a gel that does not collapse under its own weight. It also shows that a disturbed sediment regains its strength after a few weeks.

Note that the tilt was chosen to be such that air water interface is above the upper part of the sediment. The slightly denser sediment than water has a driving force to move downward and displace and "lift" the adjacent water. The force is proportional to the density difference between sediment and water. This was enough to break the strength of the sediment but only after many hours.

The situation would be different if instead of water there is air in contact with the sediment and the driving force is the full weight of sediment. The disrupting force would then be much larger. This is explored next.

Returning to #3. The tube was turned nearly horizontal and no deformation of sediment is seen. It behaves like a gel. This is shown in Figure A-4 in the left hand picture.

The tube was then tilted with bottom upward so that the air bubble is in contact with the sediment. Immediately the sediment deformed as shown in the right hand picture but it did not flow.

After a few minutes the sediment "body" split in two and the lower part slid slowly downward as shown in Figure A-5.

These results suggest that the sediments behave largely as gel that can resist gravity-induced stress, but only for hours to a day when the sediment is still quite young compared to times of interest for a repository.

Figure A-4. *Behaviour of sediment in* ***#3*** *after tilting.*

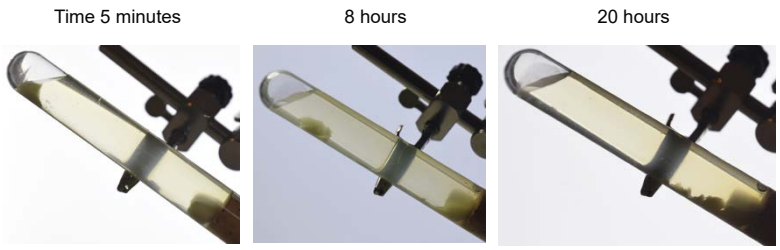

Figure A-5. *Sliding of sediment in #3 after tilting.*

A number of other simple experiments in transparent cubic $(5\ cm)^3$ jars under similar conditions but longer times support the above results. Similar experiments with a commercial mmt purified of detritus and ion exchanged to the Na form, Nanocor® PGN in 200 ml bottles show similar results. Figure A-6 shows phase separation after 91 days. These sediments also can be tilted without collapsing for days and more. Figure A-6 shows four bottles with Nanocor mmt after sedimentation for 91 days. The figures above show initial W% of the suspension for each bottle. The following lines show the W% and V% in the sediments. The Nanocor mmt formed very loose foam that did not de-areate and collapse even after prolonged vigorous shaking. This is seen at the top of the bottles in Figure A-6. The amount of mmt in the foam was estimated to be a small fraction of the original mass. No foam developed in the tests with MX-80 in the test tubes nor in the transparent jars.

The longer aging in Pujalas experiments suggests that sediment continues to grow denser with time.

A2.3 Conceptualization of expansion, solubilisation, flocculation and sedimentation

Figure A-7 illustrates a conceptualisation of the expansion, solubilisation and phase separation of originally compact mmt clay.

Compact clay expands by taking up water, **a** to **b**) by repulsive diffuse double layer, DDL, forces. When below CCC the expansion would go on indefinitely filling out all available water volume, **c** and **d**). At around 1 % by volume the thin flat colloid particles can rotate and the positively charged edges, E, by the random Brownian movement hit the negatively charges faces, F, and form EF bonds, **e**). This can be by coulombic or vdW attraction. Over time the EF groups find other EF groups and build larger and stronger 3D flocs that sediment in a gravity field and form gel. This can be visualised as a space filling cohesive house of cards, HoC, **f**. The flocculation is facilitated by gentle stirring e.g., induced by sedimenting flocs and water seeping in fractures. Actually, the EF attraction need not be only caused by coulombic bonding. When an atom belonging to the face comes very near an atom on the face, bonding could also result considering that the vdW attraction energy is proportional to the 6th power of the distance between the atoms (Israelachvili 2011). The atom to atom vdW force can be as large as the coulombic force at nm distances.

The particle density in such a structure can be estimated as well as its strength, assuming that the EF is formed by coulombic and or vdW forces. Experiments and HoC-Monte-Carlo simulations have confirmed this for synthetic Laponite clay (Ruzicka et al. 2011). See also Shalkevich et al. (2007) who discuss cluster, glass, and gel formation and viscoelastic phase separation.

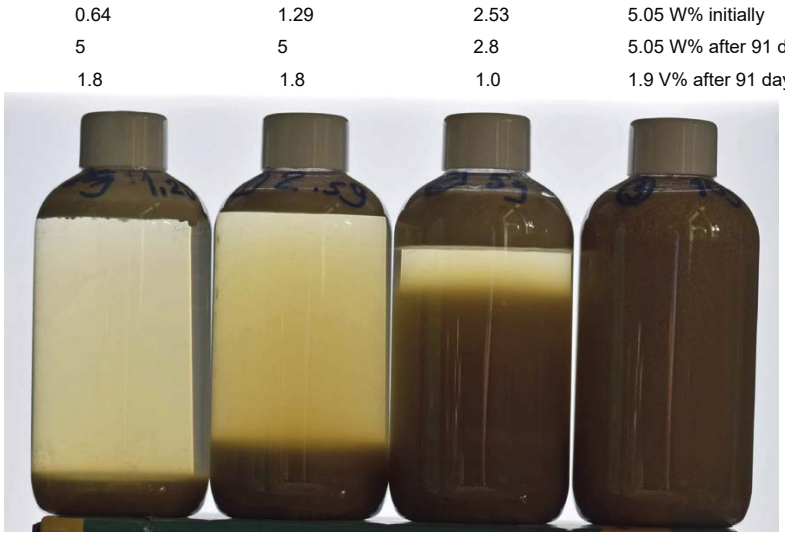

Figure A-6. *Phase separated Nanocor PGN mmt after 91 days. pH is 9.4 in the clear liquid.*

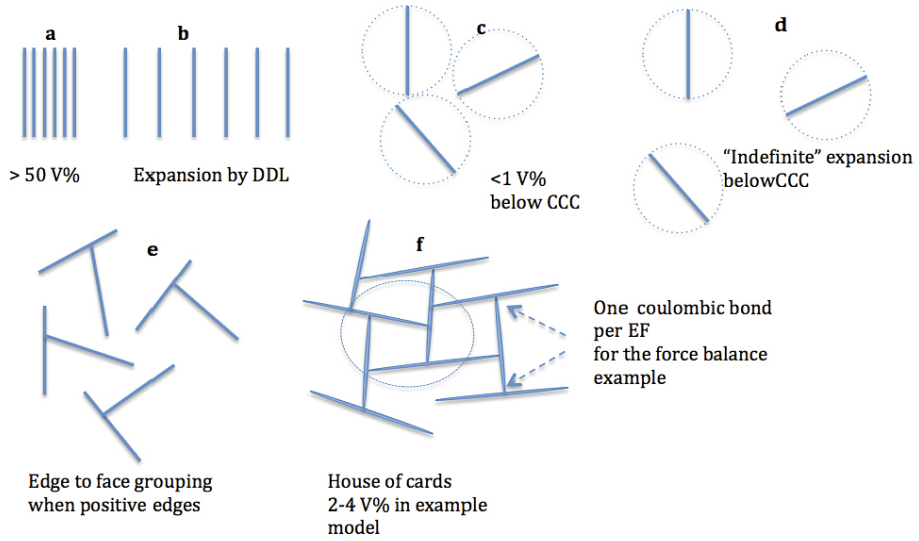

Figure A-7. *Conceptualisation of expansion, solubilisation, flocculation and phase separation of an originally compact expanding mmt clay.*

The volume fraction ϕ (or V%) of the solid platelets in the HoC is estimated in the following way. The water volume between the platelets in the 3D configuration is on the order of $V_w \approx d_p(\frac{d_p}{2})^2$ for the enclosures between six platelets. The volume V_p of the parts of the 6 platelets with thickness δ belonging to the enclosure is

$V_p \approx \frac{\left(2\left(\frac{d_p}{2}\right)^2 + 4\frac{d_p}{2}d_p\right)\delta}{2}$. The "/2" means that each side of the enclosure is shared with one neighbouring enclosure.

This gives $\phi = \frac{5\,\delta}{d_p}$. For typical platelet dimensions of mmt, δ = 1 nm and d_p = 200 nm the volume fraction ϕ = 0.025 (about 7 W%). This is surprisingly close to what was found in the scoping experiments as well as in those by Pujala (2014).

A2.4 Estimation of yield strength and minimum slot aperture for gravity induced flow

Simple experiments are used to roughly estimate the yield strength and also to assess the aperture of a vertical slot at which the AF fluid or gel could be mobilised by gravity.

When in the horizontally tilted tube the vertical boundary between the sediment and water interface stays stable the lower bound of the yield strength, τ_o, of the sediment can be roughly estimated from the pressure difference between sediment and water at the bottom of the sediment height, h_{sed}. The sediment pillar exerts a vertical pressure $\rho_{sed}\, g_c h_{sed}$. Adjacent to it is the same height of water, which presses with $\rho_w\, g_c h_{sed}$. Being fluids, albeit one is non-Newtonian, the shear strength τ_o of the sediment holds back the flow to even out the pressure difference of the two pillars. It is

$$\tau_o = (\rho_{sed} - \rho_w)\, g_c h_{sed} \qquad \text{(A-1)}$$

The density difference $(\rho_{sed} - \rho_w)$ between water and sediments that did not deform was on the order of 20 kg/m^3 and h_{sed} one to two cm. This gives τ_o to a minimum of 2–4 Pa.

When tilted in such a way that the other medium was air instead of water the density difference ($\rho_{sed} - \rho_{air}$) is about 1 000 kg/m^3. As the sediment then flowed it implies that τ_o < about 100 Pa. In a vertical water filled fracture filled with sedimenting flocs, the weight of an unconfined (not touching the walls) sediment would increase and the stress at the bottom of a few metres of sediment would be sufficient to make it start to spread sideways in the fracture. The rate of spreading in a fracture will depend on the (apparent) viscosity of the mobilised sediment and how the friction against the walls of the slot restrains the movement.

Observations in simple experiments can also be used to make a rough estimate of the apparent viscosity of the sediment. When the sliding "blob" shown in Figure A-8 has an apparent Newtonian viscosity μ_a at the shear rate that is generated by internal circulation in the blob as it moves down an inclined wall the force balance between gravity force and restraining viscous force gives

$$F_\tau = \mu_a LW \frac{du}{d\xi} = F_g = \Delta\rho\, LW\delta g Sin(\alpha) \qquad \text{(A-2)}$$

$\frac{du}{d\xi} \cong \frac{u}{\delta/2}$ is an approximation of the velocity gradient across half the blob in which the fluid circulates. δ is thickness of blob, L and W are length and width, u the sliding velocity along the wall, ξ a coordinate perpendicular to the wall, g the gravitation constant and α the angle to the horizontal. $\Delta\rho$ is the density difference between the blob and the surrounding fluid. This gives

$$\mu_a = \frac{\Delta\rho\, \delta^2 g Sin(\alpha)}{2u} \qquad \text{(A-3)}$$

In experiment **#5** it took at least 4 hours for the 8 mm high (after turning) sediment to slide down the 10 cm long tube after the tube had been turned horizontal. The velocity was about 0.6 m/day, the thickness δ was about 8 mm and $\Delta\rho$ = 20 kg/m^3. The apparent viscosity is about 900 Pas. This is nearly one million times larger than that of water. The shear rate was about 0.002 s^{-1}.

A2.5 Forces in the HoC

Within an enclosure there will be a pressure on the surface of the platelets caused by the DDL, adjacent to the charged surfaces. We illustrate this for an enclosure with side length d_p = 200 nm filled with water for two cases with NaCl solutions of 1 and 0.1 mM. The distances between the platelet in the 2D orientation is then on the order of 100 nm. See Figure A-7f. The diffuse double layer pressure on the walls is about 1 000 Pa according to the DDL forces for 0.1 mM and 10 Pa for 1 mM, (Neretnieks et al. 2009). The van der Waals attractive force between two opposing sides is negligible at this distance. In the HoC there is also DDL pressures on the same platelet from an adjacent enclosure. The DDL pressure in the adjacent enclosures can be different because the distance between the platelets in those enclosures are normally different in the stochastic structures. There then will be a net force trying to disrupt the HoC. If the EF forces are much stronger than the net DDL force the enclosure sizes can differ considerably without disrupting the structure.

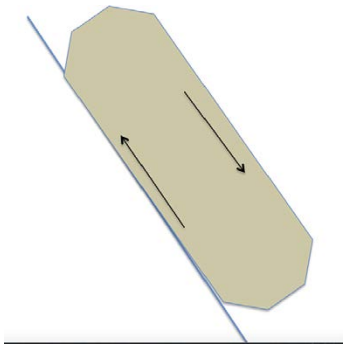

Figure A-8. *A viscous " blob" with inner circulation slides down an inclined wall.*

Assuming that there is only one bond on each of the four EF contacts of the side and that the bonds are purely coulombic, the attractive forces binding this side can be estimated by Coulombs law for two charges of opposite sign (Israelachvili 2011).

$$F = \frac{1}{4\pi\,\varepsilon_r\varepsilon_o}\,\frac{|q1 \times q2|}{r_{dist}^2} = \frac{k_e}{\varepsilon_r}\frac{|q1 \times q2|}{r_{dist}^2} \qquad \text{(A-4)}$$

ε_o is permittivity in vacuum, ε_r is relative permittivity of medium. $q1$ and $q2$ are the two charges that attract each other, r_{dist} is their distance. The charges are equal to that of one electron and are taken to be located 1 nm apart. This is approximately the size of three atom diameters. At the EF contact point one charge is located at or near the edge of the platelet and the other at a distance inside the platelet in the mid-layer of the Silicon-Aluminium-Silicon oxide configuration. This gives the distance of about r_{dist} = 1 nm between the two charges. The material between the charges is SiO_2, which has a relative permittivity of 3.9. The attractive force is 5.9×10^{-11} N. We assume in this example that a platelet is attached by one bond at each of its four sides. The area of the platelet with side length 200 nm is $(10^{-7})^2$ m^2. These bonds can restrain the pressure difference on the surface of 5 900 Pa. This suggests that the HoC can form a gel with strong, stable configurations. The HoC will not expand due to the inner DDL pressure. Even denser HoC could form if one face binds more than one particle by its edge.

Shear forces of on the order of 10 000 Pa would deform and break the fully developed HoC. In our experiments the yield strength had reached between 2 and 100 Pa after a week. However, this is a very short time for "full" formation of HoC if this were not restrained by arrested states in local free energy minima underway to the global free energy minimum.

This type of gel formation in below CCC waters is not normally reported in publications on phase diagrams of mmt colloids. See e.g. Hedström et al. (2016) who made extensive studies of mmt/water mixtures over a wide range of mmt concentrations and ionic strengths. At low W% and ionic strenght below 4–10 mM NaCl for some clays and up to several tens of mM for other clays the sols are said to be (stable) sols.

A3 Rheology of mmt suspensions

A3.1 Formation of non-Newtonian fluid

The scoping as well as the Pujala's (2014) experiments show that no phase separation occurs when starting with 3 W% suspension or higher but that sediments with on the order of 10 W% forms when starting at 2.5 W% and lower This suggests that the particles in the sediment have had the opportunity to arrange themselves in configurations that are not possible to find when starting at higher mmt concentrations than 2.5 W%. This can be understood considering that starting at higher particle concentrations the particles in the mmt stacks are still forced to be essentially parallel in the suspension by the DDL forces. This is because if two close parallel particles are forced to come closer at one end the DDL pressure increases strongly at the narrower location and counteracts the closure. At less than about 1–2 W% the particles are on the average so far from each other that they can begin to rotate and therefore come in contact and form EF bonds. This cannot occur at higher particle concentrations. This suggests that the configuration of the sediment has reached a lower free energy than what can be found starting with higher particle concentrations when EF bonds cannot form. It is therefore likely that the yield strength of aged sediments, arranged in HoC-like structures is larger than that of young suspension with the same particle concentration.

The yield strength and apparent viscosity of young mmt suspensions can potentially give a conservative estimate of the yield strength of sedimented aged flocs formed after phase separation. It can also give some indications on flow properties of a gel that has been disrupted by strong shearing that has broken the EF bonds between the particles in the gel.

A3.2 Non-Newtonian behaviour

The viscosity, μ, of Newtonian fluids is independent of the shear rate and shear stress τ. There is a simple relation between shear stress, τ, and velocity gradient $\frac{du_x}{dy}$, also called shear rate $\dot{\gamma}$.

$$\tau = -\mu \frac{du_x}{dy} = -\mu\dot{\gamma} \tag{A-5}$$

Non-Newtonian fluids for which the apparent viscosity depends on shear stress and/or shear rate are modelled with the same formalism but empirical relations for the dependence of viscosity on shear rate, shear stress and time must be determined. Such relations cannot be derived based on only fundamental physics; but valuable insights can be gained from theoretical considerations of stress-strain relations and physics and chemistry of solutions of large molecules and suspensions of particles (Bird et al. 2002). Below some commonly used empirical models that describe non-Newtonian fluid properties are presented.

A very simple and often used relation for a non-Newtonian fluid behaviour is the power law, PL.

$$\tau = -K_{PL}\dot{\gamma}^{n} \tag{A-6}$$

The apparent viscosity at a given shear rate is

$$\mu_a = K_{PL}\dot{\gamma}^{n-1} = K_{PL}\dot{\gamma}^{m} \tag{A-7}$$

For the shear thinning fluids of interest to this paper m is between −1 and −0.8, (n is between 0 and 0.2). The apparent viscosity decreases strongly with increasing shear rate.

For the present problem the dependence of $\dot{\gamma}$, τ on time is also important. The yield stress τ_o, below which the sediment/gel will not flow in the slot increases with time, but at large stress the gel liquefies. This phenomenon is observed in Bingham bodies/fluids.

The apparent viscosity of a Bingham body/fluid can be descried as follows

$$\mu_a = \infty \text{ for } \tau < \tau_o \text{ and} \tag{A-8}$$

$$\mu_a = \mu_B \text{ for } \tau \geq \tau_o \tag{A-9}$$

The Hershel-Buckley equation, in some publications called Hershel-Bulkley, for shear stress combines the properties of the power law and the Bingham models.

$$\tau = \tau_o + K_{HB}\dot{\gamma}^{nHB} \tag{A-10}$$

The apparent viscosity for this model is

$$\mu_a = \tau_o/\dot{\gamma} + K_{HB}\dot{\gamma}^{nHB-1} \tag{A-11}$$

Experimental data can often be well fitted to the PL model as well as to the H-B model. The H-B model is more useful when assessing at what shear strength the gel will be mobilised. The PL model is more useful for the flow regime. We have found only one systematic experimental investigation in dilute waters by which we mean less than 5–10 mM, for mmts that have been allowed to age before the measurements and for solid concentrations up to 6 % by weight (Pujala 2014). These are conditions of interest for the present investigation. Pujala measured yield strength and apparent viscosity of suspensions of purified sodium mmt in deionized water. The measurements were made on suspensions that had rested 1 year. The apparent viscosity increases with resting time when the solids concentration is higher than 2.5 W%. Below this concentration, viscosity is not influenced by aging. The Pujala results show a “rapid” aging already after days to weeks. The apparent viscosity increases ten to hundredfold after a few weeks.

The shear rates in Pujala's experiments covered a range 0.1 to 1 000 s^{-1} They were found to fit very well to the Herschel-Buckley model with the exponent nHB = 0.45 as well as to the PL model with *m* going from −1 to −0.8 with decreasing mmt concentration from 6 to 3 W%. Figure A-9 shows a summary of the results fitted to the experimental data for three different mmt concentrations. The left figure shows the yield strength of the suspension. The oval indicates the region of yield strength of the sediment estimated from our own, weeks to month, old phase separation experiments.

The yield stress increases with W% mmt according to

$$\tau_o = 0.2\ (cmmt)^3 \text{ (for } cmmt > 2.5 \text{ W\%)} \qquad \text{(A-12)}$$

cmmt in Equation (A-12) is the mmt concentration in 2.5 W%. The data from Paineau et al. (2011) for Wyoming mmt, gives practically the same relation but covers a somewhat lower mmt concentration region. The other three bentonites investigated by Paineau also give similar results for the freshly prepared suspensions. Birgersson et al. (2009) obtained similar results for one day aged Wyoming mmt.

From a series of pictures in Pujalas thesis of the heights of sediments formed during 3.5 years from suspensions between 0.3 to 2.5 W% the sediment concentration could be estimated to be about 6–10 W%. No yield strength measurements of the sediments are reported.

Both the H-B model and the PL model are well fitted to the data. The PL is more convenient to use for modelling flow in slots. Figure A-10 shows an example for the concentration *cmmt* = 4 W%. For the H-B model τ_o = 12.8 *Pa and nHB* = 0.45. The PL model is $\mu_a = 25\ \dot{\gamma}^{-0.86}$. The straight line is H-B and the slightly curved line is PL equation fitted to the same data. The exponent m for the 5 and 5.5 W% suspensions is 1.0, which means that it is essentially a Bingham body/fluid that has constant apparent, viscosity once mobilised.

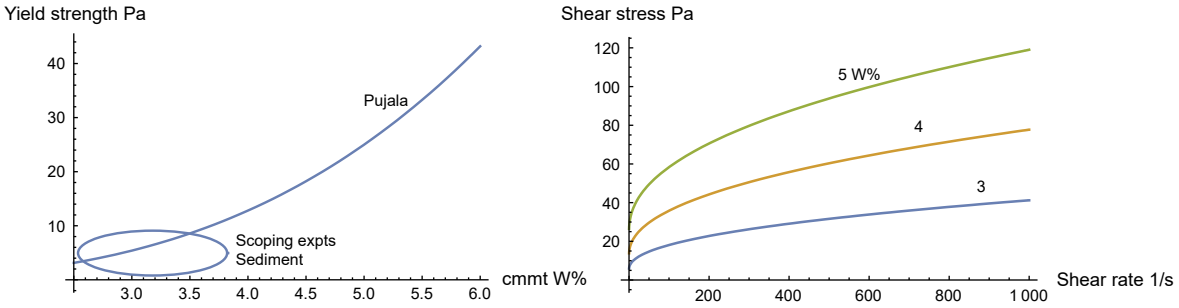

Figure A-9. *Summary of Pujala's (2014) results fitted to the Herschel-Buckley model and yield stress in the scoping experiments of sediment, the oval.*

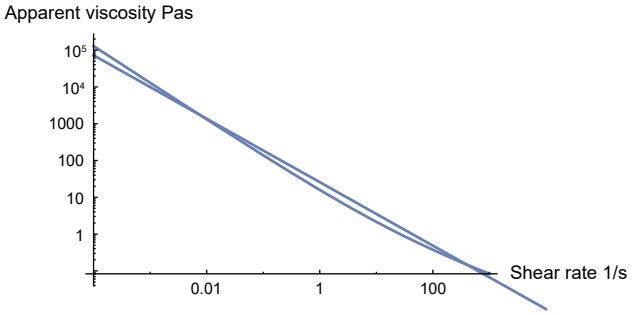

Figure A-10. *PL and H-B fitted to the same data for cmmt = 4 W%.*

A3.3 Mobilisation and flow of non-Newtonian fluid in a gravity field or by pressure gradient

When the shear stress is larger than τ_o the fluid starts to flow. It is more convenient to use the PL model because the flow equation has an exact analytical solution for this case. The H-B model is very useful to estimate when the gel starts to flow. Once mobilised the bonds in the gel have been broken and the PL-model is preferred.

The half slot aperture b_{min} that can immobilize the H-B fluid for a given pressure gradient $\frac{dP}{dZ}$ can be derived from the force balance between the force F_p generated by the pressure gradient and the friction force against the walls F_τ in the slot. L and W are slot length and width respectively.

$$F_p = W 2 b_{min} \frac{dP}{dZ} L \tag{A-13}$$

$$F_\tau = 2LW\tau_o \tag{A-14}$$

Setting the two forces equal gives

$$b_{min} = \frac{\tau_o}{\frac{dP}{dZ}} \tag{A-15}$$

In the vertical slot the pressure

$$\frac{dP}{dz} = \Delta\rho \, g_z . \tag{A-16}$$

Consider a case in which mmt has expanded from the deposition hole and released sol, separated, formed flocs, which have sedimented and after some time aged to have a yield strength. In this example the sediment has 3 W% mmt and fills a vertical fracture. gz is 9.81 m/s^2 and $\Delta\rho$ = 18.9 kg/m^3. From Equation (A-12) τ_o = 5.4 Pa and b_{min} = 2.9 cm. Thus the gel will not move in fractures with smaller aperture than 5.8 cm under its own weight.

When mobilised the flowrate in a slot with half aperture b of a PL fluid can be used to estimate the flowrate. The following relation has been derived (Bird et al. 2002, Equation 8.3-14).

The volumetric flowrate is

$$Q = \frac{2Wb^2}{\frac{1}{n}+2} \left(\frac{dP}{dz} \frac{b}{K_{PL}}\right)^{\frac{1}{n}} \tag{A-17}$$

$\frac{dP}{dz}$ is the pressure gradient.

m = −0.86 (n = 0.14) and K_{PL} = 25 Pa × s^m, taken from the example in Figure A-9.

Flow can start only when $\frac{dP}{dz} > \frac{\tau_o}{b_{min}} = \frac{12.8}{10^{-4}}$ = 0.128 MPa/m. This is a very high-pressure gradient but it could potentially be reached by the increasing swelling of the bentonite in deposition hole expanding behind the surrounding sediment. It may also be noted that τ_o increases with W% mmt and values of up to 50–100 Pa have been found (Pujala 2014, Paineau et al. 2011). This may raise the needed pressure gradient for mobilisation to about 1 MPa/m.

The flowrate "immediately" reaches on the order of 6×10^{-4} m^3/yr/m fracture width for as long as the pressure gradient is maintained at the clay/sediment interface. With increasing pressure gradient the flowrate very sharply increases proportionally to $\left(\frac{dP}{dz}\right)^{7.1}$ because of the strongly shear-thinning suspension.

A3.4 Impact of further expansion of clay from the source

The sediment cannot be mobilised in fractures smaller that 2.9 cm by the sediment gravity in the above example. As the sediment cannot move away by gravity the expanding clay behind it will start to exert a pressure on the surrounding sediment. The pressure at the swelling clay/sediment interface will increase until the pressure gradient over the sediment is sufficiently large to mobilise it as shown above. The largest mean fracture apertures expected intersecting a deposition hole is on the order of 0.1 mm. The swelling pressure of the compacted clay in the source in a KBS-3 repository is on the order of 5 MPa for a long time.

The reader is reminded that the swelling clay in the fractures may not be impeded by friction against the fracture walls in large aperture fractures because the swelling is caused by the DDL forces forcing the smectite particles apart and their rate of movement is restrained by their friction against the water moving in the other direction in the fracture to exactly replace the volume vacated by the particle with an identical volume of water (Neretnieks et al. 2009). There is thus no net movement of the clay "paste", just exchange of location between colloid particles and water. This can be seen by the analogue of two different liquids in contact with each other in a fracture, one consisting of large molecules (the colloidal particles) mixing with a small molecule liquid, water, by molecular diffusion. The *mixture* does not flow. It is just gradually diluted by water with the colloidal particles. "diluting" the water. It is so far not clear at which fracture apertures also the expanding clay will be restrained by wall friction. In contrast, the sediment-gel formed by flocculation and aging has attained yield strength and is pushed by the DDL forces at the clay/sediment interface by the expanding clay. The sediment is a gel and has no internal swelling pressure, as the swelling clay has even at the same cmmt. The sedimented gel will resist the rising pressure (stress) exerted by the expanding clay due to friction against the walls. It may possibly also be additionally compressed. The gel will be mobilised in smaller and smaller fractures as the pressure at the swelling clay/sediment interface increases. Figure A-11 shows the aperture of the fractures that can just restrain the movement for a case where the sediment has had time to develop a sediment gel a distance ΔZ in fractures. In the example we set ΔZ =1 m. The pressure driving the sediment could at most be the maximum swelling pressure of the compacted clay, 5 MPa. We also exemplify a lower value, 1 MPa.

Another way to illustrate the mobilisation is shown in Figure A-12. This shows the gradient $\Delta P/\Delta Z$ needed to mobilise a gel with τ_o = 10 Pa yield stress. In this example it is assumed that the gel is not compressible.

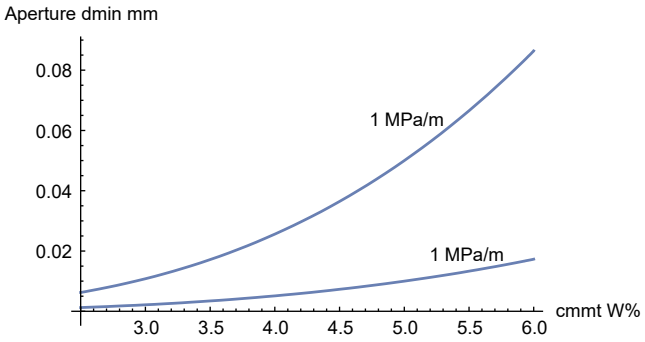

Figure A-11. *Fracture apertures in which a ΔZ = 1 m long sediment could just be mobilised for an expanding pressure of 1 and 5 MPa as function of mmt concentration.*

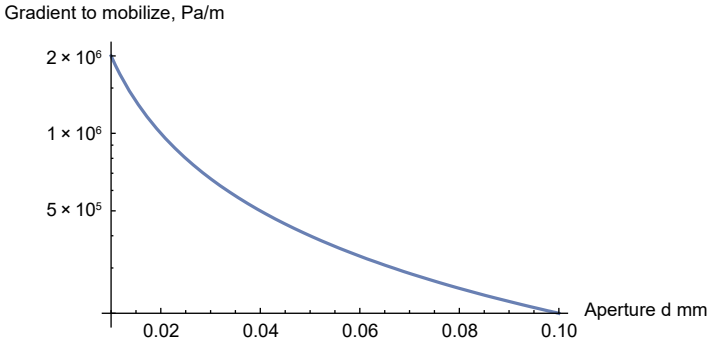

Figure A-12. *Pressure difference $\Delta P/\Delta Z$ (gradient) needed to mobilise a ΔP = 1 m thick H-B gel with 10 Pa yield stress.*

Conceptually, once the sediment has been mobilized it moves a little distance but stops because the swelling pressure of the expanding drops abruptly by its expansion at the clay/gel interface. The rate of expansion of the clay is very slow and it takes time for it to expand and again attain sufficient swelling pressure to remobilize the sediment that has had time to regain yield stress.

The rate of expansion of the rim pushing the sediment can be roughly estimated by solving the PDE equation for expansion of the clay from the deposition hole in which the swelling pressure is taken to be 5 MPa, when the pressure at the interface to the gel is at the value needed to mobilise the sediment. Such modelling can be found in Neretnieks et al. (2017). In the example we use, as before, 0.128 MPa for the 0.1 mm aperture fracture. This swelling pressure is generated by a clay at a volume fraction of 0.1 (Neretnieks et al. 2009]. Figure A-13 shows how the radius of the clay/gel interface r_R expands over time for the volume fraction $\phi_R = 0.1$ at the interface. It also shows the expansion for $\phi_R = 0.01$, which applies when the mmt at the interfaces is solubilised and is assumed to be lost by sedimentation without any need for the expanding clay to push it. The latter situation is modelled in Neretnieks et al. (2017). We conclude that unless the sediment develops a much stronger yield stress it will not seriously impede the clay expansion in fractures with apertures larger than 10 micrometre under the conditions assumed in the example. Some clay will be lost in the larger fractures.

Several questions arise around the assumed conditions. Will the gel quickly maintain or regain its original yield stress when mobilised? Will it possibly even be compressed and therefore need a larger gradient to allow the clay to expand? We have found no information in published literature that could help us to consider these situations.

A4 Clogging of pores and fractures by accessory minerals

A4.1 Detritus properties

The previous sections have described behaviour of clay that contains only colloidal size particles of mmt. Natural bentonites contain ten(s) of percent by weight of accessory minerals (detritus), some soluble, most with very low solubility. Detritus particles, even un-charged, are pushed by the DDL forces with essentially the same pressure that forces the mmt particles apart (Evans and Wennerström 1999). It is expected that detritus will move with the expanding clay until the DDL forces are too weak to push them in a gravity field. This happens when mmt is solubilised or until the detritus is strained in narrow passages.

There is mounting evidence that the detritus will build up filters at the mouths of pores and fractures in the variable aperture fractures themselves. This will eventually clog them. Figure A-14 shows the particle size distribution of detritus collected from three samples of MX-80 bentonite. They have a size distribution comparable to the aperture sizes expected intersecting deposition holes, which is less than 0.1 mm. The thin sheet-like mmt colloid particles are typically between 200 and 300 nm large.

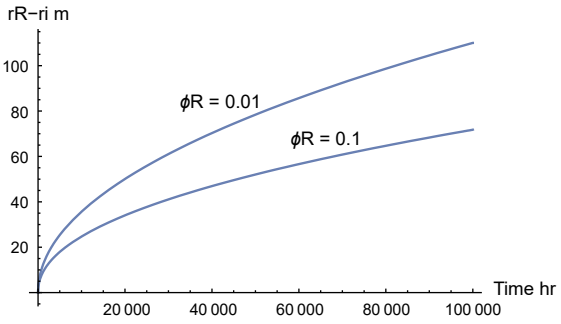

Figure A-13. *Expansion of the compacted clay in a deposition hole when pushing sediment in a 0.1 mm fracture ($\phi_R = 0.1$) and when solubilized clay "just disappears" ($\phi_R = 0.01$).*

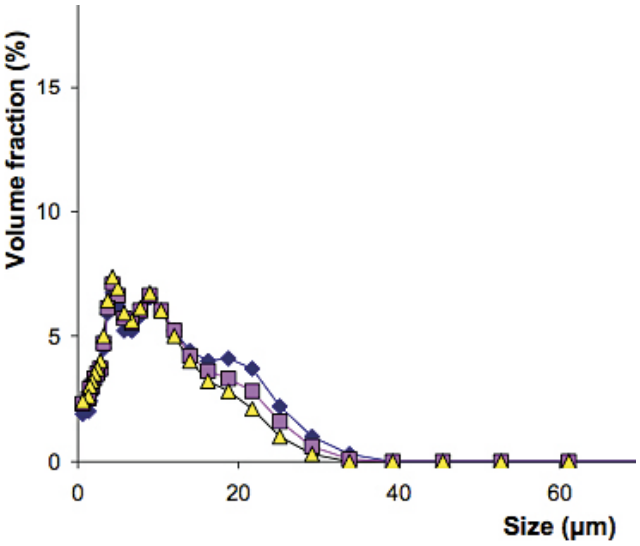

Figure A-14. *Particle size distribution for accessory particles from MX-80 from three different measurements (Richards and Neretnieks 2010).*

A4.2 Pore and fracture blocking

Fractures have variable apertures and the detritus particles driven by the expanding mmt are expected to be physically trapped in the narrow locations and gradually form blocking filters. This was demonstrated in an experiment (Reid et al. 2015), who studied clay expansion in a replica of a natural fracture and showed that a filter of the detritus formed, expanded and finally clogged the fracture. Richards and Neretnieks (2010) showed that the build-up of one to two mm thick filter-cake of detritus practically stopped further smectite particles passing through the filters.

It has been found that mmt cleaned of detritus passes 2 and 10 μm pore filters with the same ease as in larger passages but practically do not pass 0.5 μm filters, Birgersson et al. (2009) as interpreted by Neretnieks et al. (2009). It has also been demonstrated that compacted natural bentonite clays containing detritus after a short initial period (50 to 200 days) in practice stop further penetration by swelling of mmt through sintered metal filters with up to 100 μm pore size. This is illustrated in Figure A-15. Filters with 100, 10 and 2 μm pore size gave similar results provided the porosity was the same (Missana et al. 2011).

Neretnieks at al. (2017) compared the rate of smectite penetration through filters per area of pore cross section area derived from the flow-through filter experiments reported in BELBar Deliverable 2.12 with the measured rates of clay loss in experiments with clay expanding in 0.1 and 1 mm slots with seeping water by Schatz and Akhanoba (2017). The BELBaR experiments were made with clays with remaining detritus and at ionic strengths below CCC. The detritus containing material showed orders of magnitude, at later time even many orders of magnitude smaller mmt loss than the flow experiments in constant aperture slots.

We deem the above results as strong evidence that clays with detritus under below CCC ionic strength rapidly clog pores and consequently also fractures of up to 0.1 mm. These detritus filters in clogged sections will not be displaced because the particles would essentially have to be crushed to accomplish this.

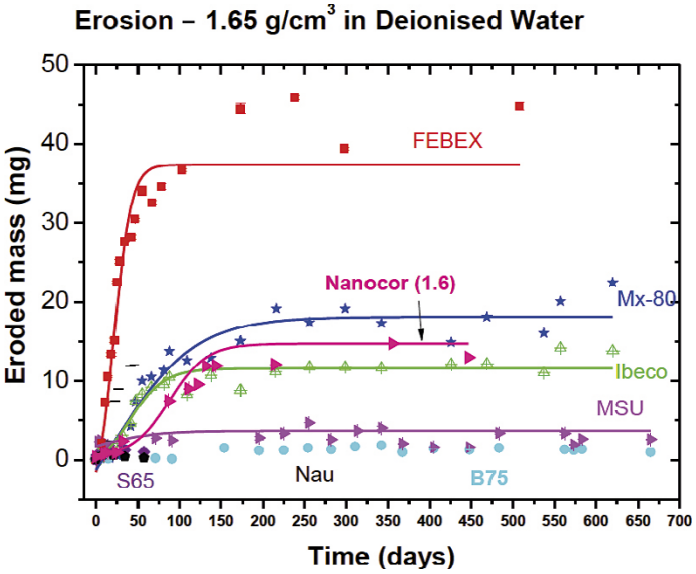

Figure A-15. *Eroded mass measured as function of time in de-ionised water from different raw bentonites compacted to 1.65 g/cm³ in non-flow tests (Schatz et al. 2015).*

A5 Discussion and conclusions

Clear evidence of phase separation of dilute mmt sols in below CCC waters has been demonstrated. The phase containing the mmt has volume fractions clearly larger than 5 W% and has yield strength, possibly more than 100 Pa, when aged. The gel can support its own weight under gravity. If and when mobilised the suspension has apparent viscosity, at low shear rates, many orders of magnitude larger than water. It will not flow in even very large fractures by its own weight. However, gel that surrounds the swelling bentonite in a deposition hole could be mobilised even in 0.1 mm aperture by the swelling pressure of the expanding bentonite in the fracture. If mobilised large amounts of bentonite could potentially be lost on the 100 000 years scale unless the fractures are clogged by the detritus material in the bentonite.

There is mounting evidence that the detritus material is likely to clog variable aperture fractures of the size expected in granitic rocks. Experiments in a replica of a granite fracture show this. Numerous experiments with filters with larger pores (up to 0.1 mm) clearly demonstrate that the filters rapidly are clogged allowing only few of the smallest mmt particles to penetrate. The loss of bentonite from deposition holes is expected to be many orders of magnitude smaller than what was earlier predicted for detritus free clays.

It should be noted, however, that the build-up of even loose clay some distance, order of meter(s) in the fractures would have a very beneficial influence on the diffusion of solutes, decreasing the release of nuclides by order to orders of magnitude compared to when the seeping water in fractures flows close to the deposition hole or other repository types with large horizontal vaults. This can be especially important for long-lived non-sorbing nuclides.

A6 Acknowledgement

The encouragement and financial support from the Swedish Nuclear Fuel and Waste management Co, SKB, is gratefully acknowledged.

Arkitektkopia AB, Bromma, 2021

SKB is responsible for managing spent nuclear fuel and radioactive waste produced by the Swedish nuclear power plants such that man and the environment are protected in the near and distant future.

skb.se